Theory of Impurity Effects on the Spin Nematic State

Junji TAKANO* and Hirokazu TSUNETSUGU

Institute for Solid State Physics, University of Tokyo, Kashiwanoha 5-1-5, Kashiwa, Chiba 277-8581

The effect of magnetic bond disorder in otherwise antiferro nematic ordered system is investigated. We introduced triangular-shaped ferromagnetic bond disorder in the S=1 bilinear-biquadratic model on a triangular lattice. It is shown that the coupling between the impurity magnetic moment and nonmagnetic excitation in the bulk yields single-moment anisotropy and long-range anisotropic interaction between impurity magnetic moments. This interaction can induce unconventional spin-freezing phenomena observed in triangular magnet, NiGa₂S₄.

KEYWORDS: antiferromagnets, triangular lattice, spin nematics, quadrupolar ordering, impurity effects, spin glass

1. Introduction

Diverse novel low-energy behaviors of geometrically frustrated magnets have attracted much attention. 1) The central issue is the possibility of a spin liquid, namely a quantum disordered state where magnetic long-range order is destroyed by frustration and quantum fluctuation.²⁾ This idea was first proposed by Anderson for a Heisenberg antiferromagnet on the triangular lattice.³⁾ Although subsequent numerical works showed the presence of magnetic long range order for that model,⁴⁾ the possibility of spin liquid states have been intensively studied, both experimentally and theoretically. Recently various compounds such as organic κ -(BEDT-TTF)₂Cu₂(CN)₃⁵⁾ and NiGa₂S₄⁶⁾ as well as $SrC_{9-p}Ga_{12-9p}O_{19}^{7)}$ are found to exhibit spin-liquid-like behaviors. In addition to their "spin liquid" states, spin glass states have been widely observed in geometrically frustrated magnets, 1) and this may be induced by a small amount of quenched disorder. These spin glass states could be ascribed to coexistence of intrinsic geometrical frustration and extrinsic frustration induced by disorder, but are not well understood theoretically. Therefore this is a challenging problem. Further it is interesting that these spin glass states are often observed to accompany spin liquid behavior. This implies that these two effects are closely related. One typical example of this coexistence is the case of the triangular lattice antiferromagnet $NiGa_2S_4$ and this is the issue of this paper.

In the layered chalcogenide NiGa₂S₄, magnetic Ni ions form a perfect triangular lattice well separated by GaS polyhedra, and therefore the Ni magnetism has a quasitwo-dimensional nature.⁶⁾ Each Ni ion has the electronic configuration of $t_{2g}^6 e_g^2$ and has spin S=1 formally with no anisotropy, which is consistent with the nearly isotropic susceptibility. Several low-temperature properties indicate that this system is a good candidate of gapless spin liquid. First, neutron scattering experiments revealed only short-range correlations of Ni spins even below ~20K. The correlation length saturates to $\xi \sim 20$ Å, corresponding to seven times the inplane lattice constant⁶⁾ and very short. Second, magnetic specific heat shows a power-law dependence $C_M \propto T^2$ in the tem-

perature regime $0.35\text{-}4\mathrm{K}$, which signals gapless and linearly dispersive modes of excitations.⁶⁾ Lastly, magnetic susceptibility approaches a finite value as temperature approaches $0\mathrm{K}$, indicating the absence of a finite spin gap.⁶⁾

To clarify the origin of this gapless "spin liquid" behavior in NiGa₂S₄, Tsunetsugu and Arikawa proposed a scenario of antiferro nematic order. This is equivalent to an antiferro spin quadrupolar (AFQ) order, where order parameters are quadrupole moments, $Q_{\mu\mu'} = \frac{1}{2} \langle S^{\mu}S^{\mu'} + S^{\mu'}S^{\mu} \rangle - \frac{1}{3}S(S+1)\delta_{\mu\mu'}$. They investigated an S=1 spin model with bilinear and biquadratic (BLBQ) couplings on the triangular lattice, defined as

$$H = \sum_{\langle i,j \rangle} \left[J \mathbf{S}_i \cdot \mathbf{S}_j + K (\mathbf{S}_i \cdot \mathbf{S}_j)^2 \right]. \tag{1.1}$$

First they showed this model has an AFQ order that fits the tripartite triangular lattice in the parameter region of 0 < J < K using mean field approximation. This mean-field ground state is represented as

$$|\Psi_{MF}\rangle = \prod_{\mathbf{R}} |S_x = 0\rangle_{A,\mathbf{R}} \otimes |S_y = 0\rangle_{B,\mathbf{R}} \otimes |S_z = 0\rangle_{C,\mathbf{R}},$$

$$(1.2)$$

where j labels three sublattices (A, B, and C) and $|S_{\alpha}=0\rangle_{i,\mathbf{R}}$ denotes the single-spin state with 0 eigenvalue of S_{α} -operator ($\alpha = x, y, or z$) at the j-sublattice site in the unit cell R. Then they studied low energy properties in the AFQ phase using a bosonic description of the excitation and obtained results qualitatively consistent with the three essential points in the experiments in NiGa₂S₄: (1) absence of magnetic long-range order; (2) nonvanishing susceptibility at zero temperature; (3) T^2 behavior of the specific heat. Läuchli et al. independently studied the ferro quadrupolar (FQ) phase in the parameter region $K < J \lesssim -2.5K$ of the same BLBQ model and obtained the results similar to the AFQ case.⁹⁾ Although these proposals are suggestive, we have to note that the origin of large effective biquadratic coupling, either positive or negative, remains to be clarified. Further, a more direct identification of quadrupolar order is desired.

Spin freezing is another unusual phenomenon observed in $NiGa_2S_4$. The magnetic susceptibility shows a kink at

 $T_f = 8.5 \text{K}$, and a small bifurcation between field cooling (FC) and zero field cooling (ZFC) values below T_f .⁶⁾ Muon spin rotation (μ SR) experiments revealed quasistatic relaxation of Ni spin below T_f .¹⁰⁾ These results suggest a spin freezing transition at T_f . However, the characteristic of the spin frozen state below T_f is remarkably different from the case of canonical spin glass materials. Slow Ni-spin fluctuations with a time scale of μ s exist and are rapidly suppressed upon application of magnetic field $\geq 10 \text{mT}.^{10}$ In order to further investigate this spin-freezing transition, Nambu et al. studied the thermodynamic properties of $Ni_{1-x}Zn_xGa_2S_4$, where Ni ions are partially replaced with nonmagnetic Zn ions.¹¹⁾ They showed that the freezing temperature T_f decreases with increasing impurity concentration x. This is just opposite to the case of canonical spin glass materials. It is also important that T_f scales with Weiss temperature, which is also the characteristic energy scale of the low temperature specific heat.

The main purpose of this paper is to propose a novel mechanism of spin freezing that is consistent with the spin liquid behavior and the unconventional spin freezing in NiGa₂S₄. Assuming the existence of the AFQ order, we will introduce impurity magnetic moments in the system and study interaction between them mediated by low energy excitation in the AFQ order. We will then discuss a possibility of spin-freezing caused by this interaction.

This paper is organized as follows. In §2, we will introduce a model for a single disorder, which induces magnetic moments in otherwise AFQ ordered system. We also describe the strategy of our calculations. In §3 we will derive effective continuum models to describe low-energy excitation in the AFQ order. Using this, we will study the one-impurity problem in §4, to investigate the coupling between an individual magnetic impurity and low-energy excitations in the bulk. In §5, we will derive interactions between the impurity magnetic moments, mediated by the low-energy bulk excitation. Then we will discuss the possibility of spin-freezing caused by this interaction in §6. Finally §7 is a short summary.

2. Model and Strategy

We start with introducing a microscopic model of $NiGa_2S_4$ including magnetic disorder, which can explain observed spin freezing, in §2.1. We mainly study the case of T=0 and our basic assumption is that the system has the AFQ order. Then we describe our basic strategy of calculations in §2.2.

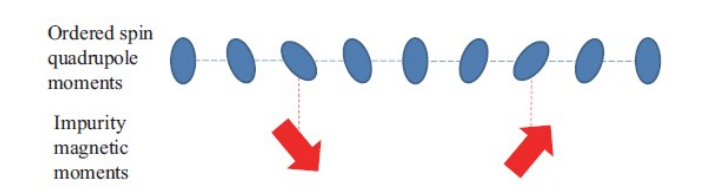


Fig. 1. Schematic diagram for the interaction between impurity magnetic moments. Dotted lines denote abstract interactions.

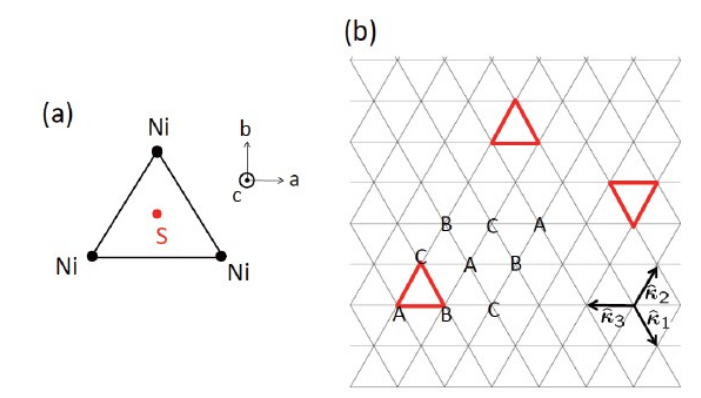


Fig. 2. (a)Position of a sulfur site in NiGa₂S₄. (b)Triangle bond disorder, three sublattices, and lattice vectors $\hat{\kappa}_i$ (i=1,2,3) defined below eq. (4.15).

2.1 Model

One feature of the spin freezing in $NiGa_2S_4$ is that the freezing temperature T_f scales with the characteristic energy scale of low-temperature specific heat, which is ascribed to collective excitations in the AFQ order. This implies that the spin freezing has close relationship with the AFQ order. We consider that the freezing is induced by the interaction between disorder-induced magnetic moments, which is mediated by low energy excitations in the AFQ order, as schematically shown in Fig. 1.

As a specific realization of this scenario, we construct a microscopic model as follows. First, for the pure bulk system to which impurities are to be introduced, we employ the BLBQ model (1.1), which is a minimal model for the AFQ order. We investigate the parameter region 0 < J < K, where the ground state has the AFQ order. Note that the bilinear interaction is rather simplified in this model. Large third-neighbor interaction is believed to exist in NiGa₂S₄,⁶⁾ but it is not included in our model. We use the model (1.1) for simplicity of the discussion. Second, we introduce disorders to the system. Here we focus on bond disorder, not site disorder, considering experimental results. Small deficiency of sulfur concentration drastically enhances the glassy behavior in hysteresis of the magnetic susceptibility. 12) Sulfur ions are located above or below the center of each triangular plaquette, as shown in Fig. 2(a), and their orbitals are in dominant exchange pathways. Disorder is induced in exchange interaction due to the vacancy of sulfur sites, and this is essential for the spin freezing behavior. Taking this into account, we introduce a different bilinear coupling for the bonds in a triangular plaquette at the impurity position. Thus, the model reads

$$H = \sum_{\langle i,j \rangle \notin D}^{n.n.} \left[J \mathbf{S}_i \cdot \mathbf{S}_j + K (\mathbf{S}_i \cdot \mathbf{S}_j)^2 \right] + \sum_{\langle i,j \rangle \in D}^{n.n.} \left[J' \mathbf{S}_i \cdot \mathbf{S}_j + K (\mathbf{S}_i \cdot \mathbf{S}_j)^2 \right], \qquad (2.1)$$

where D denotes randomly distributed triangular plaquettes and an example configuration is shown in Fig.

2(b). Hereafter we call this individual triad of disorder bonds, simply *impurity*. We assume that the biquadratic coupling K in eq. (2.1) is not affected by impurities, since we focus on the behavior of the magnetic dipole moments induced by disordered exchange couplings, while the local variation in K does not yield significant results. Further, we study the ferromagnetic case J' < 0, in which the model is consistent with the scenario above, since three spins on an impurity plaquette tend to align and form an impurity magnetic moment as a whole.

2.2 Basic Strategy

Before starting calculations, it is useful to describe the framework and limitations of the present study. Our goal is to obtain the interaction between impurities in the AFQ ordered state. These interactions arise from the interference of the modulations of the AFQ order and they have two parts. The first contribution is related to the fact that each impurity deforms the nematic order pattern in the host locally around it, and it is given by the interference of this static order parameter deformation between the impurities. The second contribution is mediated by the interactions of impurities and quantum excitations in the bulk. One impurity interacts with different sets of excitations depending on impurity magnetic state. Those excitations propagate in the bulk and interact with another impurity, which is also dependent on the magnetic state of the second impurity, and this leads to impurity-impurity interactions.

In the present study, we focus on the first contribution, i.e. the one given by static deformation of the nematic order due to impurity and neglect the contribution of dynamical quantum excitations. This may be partially justified by the fact that the AFQ order is stable in the parameter region (0 < J < K) of the BLBQ model and the reduction of the nematic order parameter due to quantum fluctuations is quite small.^{8,9)} This does not exclude the possibility that quantum fluctuations play some essential role, but this problem is beyond the scope of this study and should be examined in the future. However, based on a heuristic argument, we expect that dynamical quantum effects also lead to impurity-impurity interactions with similar nature, and we will discuss this briefly at the end of $\S 6$.

To describe static deformations of the nematic order, we employ a site-dependent mean field approximation. The phase space is restricted to the subspace of site-factorized wave functions $|\Psi_{\rm MF}\rangle = \prod_i \psi_i$ where ψ_i denotes a one-spin wave function at site i. Local nematic and magnetic order parameters are given by $Q_i^{\mu\nu} = \langle \psi_i | \frac{1}{2} (S_i^{\mu} S_i^{\nu} + S_i^{\nu} S_i^{\mu}) | \psi_i \rangle - \frac{1}{3} S(S+1) \delta_{\mu\nu}$ and $m_i = \langle \psi_i | S_i | \psi_i \rangle$ respectively, and the energy of the corresponding configuration is given by $\langle \Psi_{\rm MF} | H | \Psi_{\rm MF} \rangle$. In this way, the energy is a functional of these local fields $\{Q\}$ and $\{m\}$, and will construct a "classical" Hamiltonian describing this energy cost and its continuum limit. This is a classical model because only static deformations are considered there. Low energy configurations within this approximation are accompanied with longwavelength distortions of the order parameters, and this distortion is referred to as excitation in the following.

Within this framework, we will evaluate the energy and configuration of the ground state with two impurities. The result shows peculiar nature of impurity-impurity interaction, and this interaction is a key of novel type of spin freezing, which can describe the peculiarity of the spin freezing phenomena observed in NiGa₂S₄.

3. Continuum Theory of the Bulk

The bulk part of the model (2.1) behaves as a medium of the interaction between impurities and only low energy excitations in the AFQ order play a significant role, while detailed lattice structure is not important. It justifies replacing the bulk part with an effective field theory describing low energy excitation, and let us derive the effective model in this section. There are two kinds of excitations. One is nonmagnetic excitation corresponding to deformation of the order of spin quadrupole moments. The other is magnetic excitation, which induces magnetic dipole moments. We introduce field variables describing these excitations and derive effective models up to the second order in these fields. Up to this order, nonmagnetic and magnetic excitations are decoupled.

It is convenient to introduce the following time-reversal invariant basis for each site:¹³⁾

$$|x\rangle = i\frac{|1\rangle - |\overline{1}\rangle}{\sqrt{2}}, \ |y\rangle = \frac{|1\rangle + |\overline{1}\rangle}{\sqrt{2}}, \ |z\rangle = -i|0\rangle, \quad (3.1)$$

where $|1\rangle, |0\rangle$, and $|\overline{1}\rangle$ denote the eigenstates of S_z operator with eigenvalues 1,0, and -1 respectively. A general one-spin wave function is represented as

$$|\mathbf{d}\rangle = d_x |x\rangle + d_y |y\rangle + d_z |z\rangle, \quad \mathbf{d} \in \mathbb{C}^3$$
 (3.2)

and we define two real vectors as the real and imaginary parts of d:

$$d = u + iv, \qquad u, v \in \mathbb{R}^3.$$
 (3.3)

These vectors satisfy the normalization condition $|\boldsymbol{u}|^2 + |\boldsymbol{v}|^2 = 1$, and can also satisfy the orthogonality $\boldsymbol{u} \cdot \boldsymbol{v} = 0$ and the condition $|\boldsymbol{u}| \geq |\boldsymbol{v}|$ by choosing an appropriate phase factor. We choose a local phase satisfying these relations in the rest of this paper. Using this representation, the expectation value of the Hamiltonian (1.1) with regard to the site-decoupled wave function $|\Psi_{\rm MF}\rangle = \prod_i |\boldsymbol{d}_i\rangle$ is written as

$$\langle \Psi_{\rm MF} | H | \Psi_{\rm MF} \rangle =$$

$$\sum_{\langle ij\rangle} \left\{ (4J - 2K)[(\boldsymbol{u}_i \cdot \boldsymbol{u}_j)(\boldsymbol{v}_i \cdot \boldsymbol{v}_j) - (\boldsymbol{u}_i \cdot \boldsymbol{v}_j)(\boldsymbol{v}_i \cdot \boldsymbol{u}_j)] \right.$$

+
$$K[(\boldsymbol{u}_i \cdot \boldsymbol{u}_j)^2 + (\boldsymbol{v}_i \cdot \boldsymbol{v}_j)^2 + (\boldsymbol{u}_i \cdot \boldsymbol{v}_j)^2 + (\boldsymbol{v}_i \cdot \boldsymbol{u}_j)^2]$$
.

On the basis of this expression, we will derive the effective model for nonmagnetic excitation in §3.1 and then will turn to the effective model for magnetic excitation in §3.2.

3.1 Effective Model for Nonmagnetic Excitation

Let us derive the effective model for nonmagnetic excitation first. This describes the energy of configurations under the condition that the magnetic moment $\mathbf{m} = 0$ at any site. We will show the effective model is the O(4)

nonlinear- σ model. Since the magnetic moment is given by $\boldsymbol{m} = \langle \boldsymbol{S} \rangle = 2\boldsymbol{u} \times \boldsymbol{v}$, the condition $\boldsymbol{m} = 0$ corresponds to $|\boldsymbol{u}| = 1$ and $\boldsymbol{v} = 0$. In this case one-spin state is characterized by vector \boldsymbol{u} , referred to as director. Note that this representation is double-valued. Two states with directors $\pm \boldsymbol{u}$ differ only by a phase factor and hence correspond to the identical physical state. The Hamiltonian (3.4) becomes

$$H = \sum_{\langle ij \rangle} K(\boldsymbol{u}_i \cdot \boldsymbol{u}_j)^2. \tag{3.5}$$

In the ground state of the disorder-free bulk system, directors in each sublattice are spatially uniform and orthogonal between different sublattices. Nonmagnetic excitations mean a long-wavelength distortion of this set of ordered directors. Hence, as a local order parameter, we can use an orthogonal triad of unit vectors, which corresponds to the directors at mutually nearest neighbor sites belonging to the three sublattices. Strictly speaking, the orthogonality of the directors between nearest neighbor sites can be slightly violated, but we can ascribe this deviation to spatial variation of the local order parameter. We represent this triad as a SO(3), or almost equivalently a SU(2) rotation operation, and here we choose the latter for convenience. This representation has multivalueness since the directors are double-valued and also each SO(3) matrix has double representation in SU(2). Although such redundancy plays an essential role for topological excitation, it is not relevant to the effects of spin-wave like excitation, which is studied in this paper. (We will summarize the properties of topological excitation in this system in Appendix B, and the important point is that the non-Abelian fundamental group of the AFQ order parameter implies a nontrivial merging rule of topological excitations.) Therefore, we hereafter use the spin-1/2 representation of the SU(2) group, i.e. SU(2) matrix. Due to the locality and the SU(2) invariance, we can expect the effective model will have a following form,

$$H^{\pi} = \frac{J_{\pi}}{2} \int d\mathbf{r} \operatorname{Tr} \left[\nabla U^{\dagger}(\mathbf{r}) \cdot \nabla U(\mathbf{r}) \right], \qquad (3.6)$$

with SU(2) field variable $U(\mathbf{r})$ and stiffness constant J_{π} . After a standard parametrization, this model is mapped to the O(4) nonlinear- σ model. Let us now derive this effective continuum model from the lattice model (3.5) and also determine the value of J_{π} . We construct the correspondence between the triad and the matrix as follows. First we define a double-valued unit vector $\boldsymbol{\xi}(\boldsymbol{x}_i)$, $\boldsymbol{\eta}(\boldsymbol{x}_i)$, or $\boldsymbol{\zeta}(\boldsymbol{x}_i)$ depending on sublattice as

$$\xi(\mathbf{x}_i) = \pm \mathbf{u}_i \quad i \in A, \ \eta(\mathbf{x}_i) = \pm \mathbf{u}_i \quad i \in B,$$

$$\zeta(\mathbf{x}_i) = \pm \mathbf{u}_i \quad i \in C.$$
 (3.7)

Under appropriate choices of signs, all vectors vary in space slowly compared with the lattice constant in the low energy sector. Then we extend these vectors by interpolation to those defined for continuous spatial coordinate \mathbf{r} and impose the orthogonality among the three fields. Lastly we define the SU(2) field variable $U(\mathbf{r})$ by

$$U(r)\chi[x] = \chi[\xi(r)], \ U(r)\chi[y] = \chi[\eta(r)],$$

$$U(r)\chi[z] = \chi[\zeta(r)], \tag{3.8}$$

where $\boldsymbol{x} = (1,0,0), \ \boldsymbol{y} = (0,1,0), \ \boldsymbol{z} = (0,0,1), \text{ and } \boldsymbol{\chi}[\boldsymbol{N}]$ denotes the two component spinor representation of the spin 1/2 coherent state¹⁴⁾ corresponding to the unit vector \boldsymbol{N} :

$$\chi[N] = \begin{pmatrix} \cos\left(\frac{\theta}{2}\right) \exp\left(-\frac{i\phi}{2}\right) \\ \sin\left(\frac{\theta}{2}\right) \exp\left(+\frac{i\phi}{2}\right), \end{pmatrix}$$
(3.9)

using polar coordinates as $N=(\sin\theta\cos\phi,\sin\theta\sin\phi$, $\cos\theta)$. It is known that a SU(2) matrix is written with four real parameters as

$$U(\boldsymbol{r}) = \pi_0(\boldsymbol{r}) + \sum_{j=1}^3 i \tau_j \pi_j(\boldsymbol{r})$$

$$\pi_{\mu} \in \mathbb{R}, \quad (\mu = 0, 1, 2, 3), \quad \sum_{\mu=0}^{3} \pi_{\mu}^{2} = 1,$$
(3.10)

where τ_j 's(j = 1, 2, 3) are Pauli matrices. Hereafter we regard π_{μ} 's $(\mu = 0, 1, 2, 3)$ as local order parameters.

Next we rewrite the bond Hamiltonian (3.5) in terms of the field variables $\pi_{\mu}(\mathbf{r})$. We can derive straightforwardly the representation of the continuated director vectors, $\boldsymbol{\xi}(\mathbf{r})$, $\boldsymbol{\eta}(\mathbf{r})$, and $\boldsymbol{\zeta}(\mathbf{r})$, such as

$$\boldsymbol{\xi} = (\pi_0^2 + \pi_1^2 - \pi_2^2 - \pi_3^2, 2(\pi_1 \pi_2 - \pi_0 \pi_3),$$
$$2(\pi_0 \pi_2 + \pi_1 \pi_3)). \tag{3.11}$$

Using these relations, and rewriting $\pi(x_i)$ and $\pi(x_j)$ as π , and $\pi + \delta \pi$ respectively, we have interaction

$$H_{ij} = 4K \left(-\pi_3 \delta \pi_0 - \pi_2 \delta \pi_1 + \pi_1 \delta \pi_2 + \pi_0 \delta \pi_3 \right)^2$$

$$\equiv H_{AB}(\mathbf{r}, \mathbf{r} + \delta \mathbf{r}), \tag{3.12}$$

between the sites i and j when $i \in A, j \in B$. We similarly define H_{BC} and H_{CA} .

Summing over all the site pairs and taking the continuum limit, we obtain the O(4) nonlinear- σ model as the effective model for nonmagnetic excitations, as we expected in eq. (3.6).

$$H^{\pi} = \frac{1}{2} J_{\pi} \sum_{\mu=0}^{3} \int d\mathbf{r} (\nabla \pi_{\mu})^{2}, \qquad \sum_{\mu=0}^{3} \pi_{\mu}^{2} = 1, \quad (3.13)$$

where $J_{\pi} = (8/\sqrt{3})K$. As shown by Polyakov and Wiegmann, this model is identical to the phenomenologically introduced effective model (3.6),¹⁵⁾ and the value of the coupling constant J_{π} is determined explicitly. This classical model describes long-wavelength distortion of the AFQ order, which physically corresponds to the energy cost of instantaneous deformation. (16) Note that the order parameter space SU(2) reflects the character of antiferro order. Due to the orthogonality of directors between different sublattices, there are locally three independent directions of distortion of the order, which correspond to rotations of ordered moments around three axes in the spin space. On the other hand, in the ferro quadratic order where directors point to the same direction regardless of sublattice, with the rotation around the director the order remains unchanged and the number of independent directions of distortion is two. Therefore we can easily conclude the effective model for the ferro quadratic order is O(3) nonlinear- σ model.

Finally we introduce further simplification for the effective model. We describe the ground state of the pure bulk as $\pi_0 = 1$, $\pi_a = 0$, (a = 1, 2, 3). Even in the presence of an impurity, the bulk region is close to this ground state. Hence we assume $|\pi_a| \ll \pi_0 \sim 1$, (a = 1, 2, 3). Expanding the effective model (3.13) in terms of the field variables π_a (a = 1, 2, 3) and preserving only the lowest order terms of π_a , we obtain the three-component massless Gaussian model:

$$H^{\pi} = \frac{1}{2} J_{\pi} \sum_{a=1}^{3} \int d\mathbf{r} (\nabla \pi_a)^2$$
 (3.14)

Note that contribution of π_0 is $O(\pi_a^4)$ and therefore neglected here. We will use this effective model to study nonmagnetic excitations afterwards. This simplification of the model is not appropriate for investigating the excitations where π -field configuration strongly deviates from that in the ground state. For example, at finite temperatures, the long range order is destroyed as manifested by Mermin-Wagner theorem, ¹⁷⁾ and the π -field varies in space among the whole parameter space even without disorders. To deal with such a situation, we have to go back to the original model (3.13).

3.2 Effective Model for Magnetic Excitation

Now we turn to derive an effective model for magnetic excitation, which will be identified as a three-component massive Gaussian model. In contrast to its nonmagnetic partner, this describes the energy of configuration without nonmagnetic excitation. This condition means that the directions of the directors \boldsymbol{u} do not change from those in the bulk ground state, while $|\boldsymbol{u}|$ can be smaller than the bulk value, $|\boldsymbol{u}|=1$. Hence we can impose

$$u_i/\!\!/x$$
 $(i \in A), u_i/\!\!/y$ $(i \in B), u_i/\!\!/z$ $(i \in C).$ (3.15)

First let us introduce field variables describing magnetic excitation. Basically we can choose three components of magnetic moments as the field variables in concern, but we have to pay attention to the following two points. First, condition (3.15) yields a restriction of magnetic moments. For example, in the A sublattice, the magnetic moment is restricted in the YZ plane, $\boldsymbol{m} = \left(0, m_2^{(A)}, m_3^{(A)}\right)$, since $\boldsymbol{m} = 2\boldsymbol{u} \times \boldsymbol{v}$. Second, coupling between magnetic moments is ferromagnetic or antiferromagnetic, depending on the parameter J/K. It is clarified by transforming the total Hamiltonian (3.4) to the form

$$\langle H_{ij} \rangle = \left(J - \frac{1}{2} K \right) \boldsymbol{m}_i \cdot \boldsymbol{m}_j$$

+ $K \{ (\boldsymbol{u}_i \cdot \boldsymbol{u}_j)^2 + (\boldsymbol{v}_i \cdot \boldsymbol{v}_j)^2 + (\boldsymbol{u}_i \cdot \boldsymbol{v}_j)^2 + (\boldsymbol{v}_i \cdot \boldsymbol{u}_j)^2 \}.$ (3.16)

The interaction between \mathbf{m}_i and \mathbf{m}_j is ferromagnetic (antiferromagnetic) when 0 < J < K/2 (K/2 < J < K). Taking these points into account, we choose field variables as follows. In the ferromagnetic region 0 < J < K/2, the three variables are defined as $\psi_1 = \frac{1}{2}m_1^{(B)} = \frac{1}{2}m_1^{(B)}$

 $\frac{1}{2}m_1^{(C)}, \psi_2=\frac{1}{2}m_2^{(C)}=\frac{1}{2}m_2^{(A)},$ and $\psi_3=\frac{1}{2}m_3^{(A)}=\frac{1}{2}m_3^{(B)}$ (here the subscript denotes a component, not a site), which correspond to "uniform" magnetizations, as the field variables varying gradually in space. In contrast, in the antiferromagnetic region K/2 < J < K, the field variables are $\psi_1=\frac{1}{2}m_1^{(B)}=-\frac{1}{2}m_1^{(C)}, \ \psi_2=\frac{1}{2}m_2^{(C)}=-\frac{1}{2}m_2^{(A)},$ and $\psi_3=\frac{1}{2}m_3^{(A)}=-\frac{1}{2}m_3^{(B)}$, which represent "staggered" magnetizations.

Next we express the Hamiltonian in terms of the field variables ψ and derive an effective model. Using the field variables defined above, the Hamiltonian (3.4) is written as:

$$H = \sum_{i \in A, j \in B, k \in C}^{\text{n.n.}} (H_{ij} + H_{jk} + H_{ki})$$
 (3.17)

$$H_{ij} = -|4J - 2K|\psi_{3,j}\psi_{3,i} + K(\psi_{3,j}^2 + \psi_{3,i}^2)$$
 etc. (3.18)

As in the previous discussion for the nonmagnetic part, we take the continuum limit, and the result is the threecomponent Gaussian model with mass terms:

$$H^{\psi} = \frac{1}{2} J_{\psi} \sum_{a=1}^{3} \int d\mathbf{r} \left[(\nabla \psi_{a})^{2} + (k_{\psi})^{2} \psi_{a}^{2} \right], \qquad (3.19)$$

where the coupling constants are given by

$$J_{\psi} = \frac{2}{\sqrt{3}}|K - 2J|, \ k_{\psi} = \frac{2}{l_0}\sqrt{\frac{K}{|K - 2J|} - 1},$$
 (3.20)

where l_0 denotes the lattice constant. Hereafter we take $l_0=1$ for simplicity. The effective model (3.19), is massive, reflecting short-range nature of magnetic correlations of the AFQ order. Note that the "mass" k_{ψ} vanishes as we approach the boundaries of the AFQ phase, J=0, or K. This singularity implies that the system becomes unstable against magnetic excitation, and manifests the onset of a magnetically ordered state. Actually, the mean-field ground state has ferromagnetic order for J<0, and 120 degree antiferromagnetic order for J>K.

4. One Impurity Problem

In this paper, we want to calculate interaction between two impurities in the AFQ order, and this interaction is mediated by coupling of each impurity and bulk excitations. Therefore, our next task is to study the problem of single impurity and calculate its coupling constant of the interaction with nonmagnetic and magnetic excitations in the bulk studied in the last section. The most important result is that induced nonmagnetic excitation field shows a power-law decay in space, much more extended than magnetic excitation field.

Our strategy is as follows. For the bulk part we use the continuum theory developed in the last section, while we use the original spin variables for the impurity part. We then derive the bulk-impurity coupling by evaluating the energy on the bonds connecting these two parts.

At this point we explain our nomenclature concerning the sites and bonds. We denote sites in the impurity as "core" sites, and sites on the border of the bulk which are connected with core sites by bonds as "shell" sites.

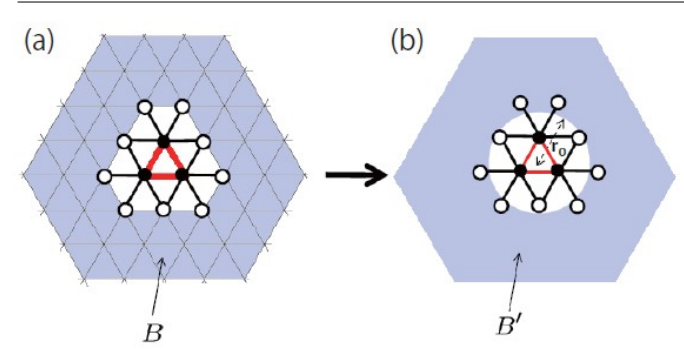


Fig. 3. Simplification of the one-impurity Hamiltonian. (a) Black (white) circles denote core (shell) sites. (b)The bulk is replaced by a continuum media and its inner boundary is approximated by a circle.

They are shown as black and white circles respectively in Fig. 3(a). We call the other sites "bulk" sites. Further we call bonds connecting core sites and shell sites (two core sites) "core-shell" ("core-core") bonds, which correspond to red (black) bonds in Fig. 3(a). Finally we call the other bonds "bulk" bonds, which are shown as gray bonds in the figure.

First, we represent states on shell and bulk sites using the two vector field variables π and ψ defined in the last section, instead of original spin wavefunctions. For core sites, we keep using original spin wavefunctions. Next, we evaluate the energy of bulk bonds using the effective massless and massive Gaussian models derived in the last section, whereas energy of core-core and core-shell bonds are evaluated for the original lattice model (1.1). In doing this, spin wavefunction at a shell site is determined by the field variables at its position. Then, we approximate the boundary of the bulk part, which has a polygon shape in the original lattice model, by a circle of radius r_0 , to make it easier to evaluate the energy of the bulk part. Finally, we consider only the dominant components of spatial fluctuations of the fields.

For simplicity, we take the limit $J' \to -\infty$ i.e. the magnetic interaction between core sites is ferromagnetic one of infinite strength. In this limit, spins on three core sites are completely polarized and described by the identical magnetic moment vector of unit length $\boldsymbol{m}, \ |\boldsymbol{m}| = 1$. We change \boldsymbol{m} and clarify the anisotropy of the magnetic moment. We will show later, using numerical calculations, that the cases of finite J' (J' < 0) are qualitatively similar to this limit.

The total Hamiltonian is

$$H = H_{\text{bulk}}^{\pi} + H_{\text{bulk}}^{\psi} + H_{\text{imp}}, \tag{4.1}$$

where $H_{\rm bulk}^{\pi}$ and $H_{\rm bulk}^{\psi}$ are the effective Hamiltonians for the normagnetic and magnetic excitations (3.14) and (3.19), and $H_{\rm imp}$ denotes the bond Hamiltonians on coreshell bonds. $H_{\rm imp}$ represents impurity-bulk interaction and is a function of the magnetic moment \boldsymbol{m} of core sites and the field variables $\boldsymbol{\pi}$ for nonmagnetic excitation and $\boldsymbol{\psi}$ for magnetic excitation on shell sites.

First we will derive $H_{\rm imp}$ perturbatively with regard to π and ψ up to the second order in §4.1. Then, we will consider only the first order term within $H_{\rm imp}$ and

examine the magnetic anisotropy. At this order we can decouple the total Hamiltonian (4.1) into nonmagnetic part H^{π} and magnetic part H^{ψ} . We will treat them separately in §4.2 and §4.3, respectively. Next we will further include the second order term and refine the anisotropy. Since we can not decouple the Hamiltonian as before, we will treat the whole Hamiltonian of this order in §4.3. Finally we will approach this problem numerically and compare the results with analytical ones in §4.4.

4.1 Perturbative Expansion of the Impurity-Bulk Interaction

Following the strategies mentioned above, firstly we expand the impurity-bulk interaction H_{imp} with regard to the two field variables, $\boldsymbol{\pi}$ and $\boldsymbol{\psi}$. An individual bond Hamiltonian $H_{\text{imp},j}$, connecting the core site i and the shell site j, is written in terms of the impurity magnetic moment \boldsymbol{m} , and the field variables on j site: $\boldsymbol{\pi}_j$ and $\boldsymbol{\psi}_j$, up to the second order of $\boldsymbol{\pi}_j$ and $\boldsymbol{\psi}_j$. Here we explain for the case where the site j belongs to A sublattice.

If there is no nonmagnetic excitation at a shell site, we can derive the correspondence between the two vectors $(\boldsymbol{u} \text{ and } \boldsymbol{v})$ and the field of magnetic excitation $\boldsymbol{\psi}$, from the definition of $\boldsymbol{\psi}$. As mentioned before, nonmagnetic excitation corresponds to rotation of local nematic order in the spin space. The directions of principal axes are given by the representation of the directors, eq. (3.11), from which we can identify the rotation matrix. Thus we represent \boldsymbol{u} and \boldsymbol{v} , in terms of both magnetic and nonmagnetic excitation:

$$\mathbf{u} = (1 - 2(\pi_1^2 + \pi_2^2) - \frac{1}{2}(\psi_3^2 - \sigma \psi_2^2),$$

$$2(\pi_1 \pi_2 - \pi_3), 2(\pi_2 + \pi_1 \pi_3))$$
(4.2)

$$\mathbf{v} = (2\pi_3\psi_3 - 2\pi_2\sigma\psi_2, \psi_3 - 2\pi_1\sigma\psi_2, -\sigma\psi_2 - 2\pi_1\psi_3),$$
(4.3)

where the third and higher order terms are omitted and $\sigma = +1$ (-1) for J < K/2 (J > K/2). As for the core site i with magnetic moment \boldsymbol{m} , we can readily obtain the value of \boldsymbol{u} and \boldsymbol{v} , from the relations among these three vectors: $|\boldsymbol{u}|^2 + |\boldsymbol{v}|^2 = 1$, $\boldsymbol{u} \cdot \boldsymbol{v} = 0$, and $\boldsymbol{m} = 2\boldsymbol{u} \times \boldsymbol{v}$. Combining these results with the bond Hamiltonian in eq. (3.4), we obtain the representation of $H_{\text{imp},j}(\boldsymbol{m}, \boldsymbol{\pi}(\boldsymbol{x}_j), \boldsymbol{\psi}(\boldsymbol{x}_j))$ for $j \in A$.

$$H_{\text{imp},j} = H_{\text{imp},j}^{\pi} + H_{\text{imp},j}^{\psi} + H_{\text{imp},j}^{\pi^{2}} + H_{\text{imp},j}^{\psi^{2}} + H_{\text{imp},j}^{\pi\psi}$$
(4.4)

$$H_{\text{imp},j}^{\pi} = 2K\epsilon_{1ab}m_1m_a\pi_b(\boldsymbol{x}_j) \tag{4.5}$$

$$H_{\text{imp},j}^{\psi} = (2J - K) \left[-\sigma m_2 \psi_2(\boldsymbol{x}_j) + m_3 \psi_3(\boldsymbol{x}_j) \right]$$
 (4.6)

$$H_{\text{imp},j}^{\pi^2} = 2K \left\{ m_1^2 \left[\boldsymbol{\pi}^2(\boldsymbol{x}_j) - \pi_1^2(\boldsymbol{x}_j) \right] - \left[\epsilon_{1ab} m_a \pi_b(\boldsymbol{x}_j) \right]^2 \right\}$$

$$(4.7)$$

$$H_{\text{imp},j}^{\psi^2} = \frac{K}{2} \left\{ m_1^2 \left[\psi^2(\boldsymbol{x}_j) - \psi_1^2(\boldsymbol{x}_j) \right] - \left[\epsilon_{1ab} m_a \psi_b(\boldsymbol{x}_j) \right]^2 \right\}$$
(4.8)

$$H_{\mathrm{imp},j}^{\pi\psi} = 2(2J - K) \left[m_1 \epsilon_{1ab}^{(\sigma+1)/2} \pi_a(\boldsymbol{x}_j) \psi_b(\boldsymbol{x}_j) + \right.$$

$$\pi_1 \epsilon_{1ab} m_a \psi_b(\boldsymbol{x}_i)], \tag{4.9}$$

where ϵ_{ijk} is Levi-Civita tensor, and summation with regard to repeatedly appearing indices is implicitly taken. This derivation for the other sublattices is straightforward and we obtain the results by changing the indices of m, π , and ψ in a cyclic way: $1 \to 2$, $2 \to 3$, $3 \to 1$, $(j \in B)$, $1 \to 3$, $2 \to 1$, $3 \to 2$, $(j \in C)$. Finally the total contribution of all the shell sites is

$$H_{\text{imp}}^{I} = \sum_{j \in \text{shell}} H_{\text{imp},j}^{I} \qquad (I = \pi, \psi, \pi^{2}, \psi^{2}, \pi\psi).$$
 (4.10)

4.2 First Order Effect of the Interaction between the Impurity and Nonmagnetic Excitation

At this point we focus on the coupling between the impurity magnetic moment and nonmagnetic excitation in the bulk region. In the impurity-bulk interaction $H_{\rm imp}$, we examine here only the first order term with regard to nonmagnetic excitation π , given by eq. (4.5). The total Hamiltonian becomes

$$H^{\pi} = H_{\text{bulk}}^{\pi} + H_{\text{imp}}^{\pi}, \ H_{\text{bulk}}^{\pi} = \frac{1}{2} J_{\pi} \sum_{a=1}^{3} \int' d\mathbf{r} (\nabla \pi_a)^2,$$

$$(4.11)$$

where \int' denotes integration over the bulk region B' with a circular void shown in Fig. 3, i.e. $\int' d\mathbf{r} = \int_{r_0}^{\infty} dr \int_0^{2\pi} d\theta$.

As mentioned before, we consider only the dominant component of the spatial fluctuation of π . This means as follows: As is clear from H_{bulk}^{π} (3.14), the ground state configuration of π satisfies the Laplace equation $\nabla^2 \pi_a = 0$, (a = 1, 2, 3), and therefore can be expanded in the polar coordinate system as

$$\pi_a(r,\theta) = \sum_{n=1}^{\infty} \left\{ c_n^{(a)} r^{-n} \cos[n(\theta - \theta_{0,n}^{(a)})] \right\}, \qquad (4.12)$$

where we impose the boundary condition $\pi_a(\boldsymbol{x}) \to 0$ with $|\boldsymbol{x}| \to \infty$. The dipole component $c_1^{(a)}$ becomes dominant as $|\boldsymbol{x}| \to \infty$, and we neglect the other components $c_n^{(a)}$, (n>1). Hereafter we call this simply "dipole approximation". In this approximation, the field variable π is given by

$$\pi_a(r,\theta) \equiv \frac{r_0 \boldsymbol{\mu}_a^{\pi} \cdot \boldsymbol{r}}{r^2},\tag{4.13}$$

where we introduced a dipole moment μ_a^{π} and its value will be determined afterward. Recall that r_0 is the radius of the circular void of the bulk region. The bulk part of the ground state energy becomes

$$E_{\text{bulk}}^{\pi} = \frac{1}{2}\pi J_{\pi} \sum_{a} (\boldsymbol{\mu}_{a}^{\pi})^{2}.$$
 (4.14)

Let us study the ground state of the total Hamiltonian (4.11), in the dipole approximation. To be specific, we consider the case that the impurity is located at position E in Fig. 4. The other cases will be summarized in Appendix A. By straightforward calculation, we find that the energy of the lattice part Hamiltonian H_{imp}^{π} has

a simple form:

$$E_{\rm imp}^{\pi} = -\frac{48}{7} K \sum_{a,b,c=1}^{3} \frac{|\epsilon_{abc}|}{2} m_b m_c \hat{\kappa}_a \cdot \mu_a^{\pi}, \qquad (4.15)$$

where $\hat{\boldsymbol{\kappa}}_a$'s are lattice vectors: $\hat{\boldsymbol{\kappa}}_1 = (1/2, -\sqrt{3}/2), \ \hat{\boldsymbol{\kappa}}_2 = (1/2, \sqrt{3}/2), \ \hat{\boldsymbol{\kappa}}_3 = (-1, 0), \text{ shown in Fig. 2(b)}.$

The total energy is the sum of the bulk part (4.14) and the impurity part (4.15):

$$E = \frac{\pi J_{\pi}}{2} \sum_{a} (\mu_{a}^{\pi})^{2} - \frac{48}{7} K \sum_{abc} \frac{|\epsilon_{abc}|}{2} m_{b} m_{c} \hat{\kappa}_{a} \cdot \mu_{a}^{\pi}$$
 (4.16)

The dipole moments are determined by minimizing this energy with respect to μ_a^{π} and the result is

$$\boldsymbol{\mu}_a^{\pi} = \mu_0^{\pi} \sum_{b,c} \frac{|\epsilon_{abc}|}{2} m_b m_c \hat{\boldsymbol{\kappa}}_a, \tag{4.17}$$

where $\mu_0^{\pi} = 48Kr_0/(7\pi J_{\pi})$. The ground-state energy is

$$E_0^{\pi}(\mathbf{m}) = \frac{1}{4}\pi J_{\pi}(\mu_0^{\pi})^2 \left(m_1^4 + m_2^4 + m_3^4 - 1\right). \tag{4.18}$$

This expression reveals that the impurity magnetic moment has an anisotropy. There are four easy axes $\frac{1}{\sqrt{3}}(1,\pm 1,\pm 1)$. Note that these directions should be considered relative to the principle axes of the local AFQ order, not to the spatial directions of the triangular lattice. Since the Hamiltonian (2.1) is SU(2) invariant, we can interpret this anisotropy as a result of SU(2) symmetry breaking in the AFQ phase.

The anisotropy energy (4.18) can also be represented as

$$E_0^{\pi}(\mathbf{M}) = -2\pi J_{\pi}(\mu_0^{\pi})^2 (M_{xy}^2 + M_{yz}^2 + M_{zx}^2), \quad (4.19)$$

using t_{2g} part of spin quadrupole moment of each impurity spin

$$M_{\alpha\beta} \equiv \frac{1}{2} \langle S^{\alpha} S^{\beta} + S^{\beta} S^{\alpha} \rangle \quad (\alpha, \beta = x, y, z, \ \alpha \neq \beta),$$
(4.20)

since $M_{\alpha\beta} = m_{\alpha}m_{\beta}/2$ is satisfied for a fully polarized spin with S = 1. We can naturally understand this by noticing that the nonmagnetic excitation π linearly couples to the spin quadrupole moment $M_{\alpha\beta}$ in the first order coupling (4.5) considered here.

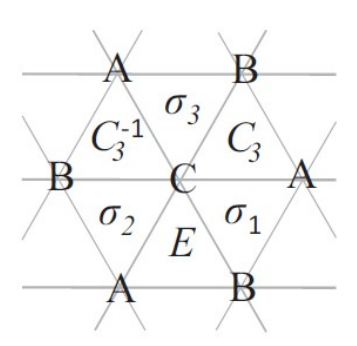


Fig. 4. Six distinct possibilities of the position of the impurity. The position "E" is chosen as reference, while the other cases may be reproduced by applying a point group operation shown in the figure.

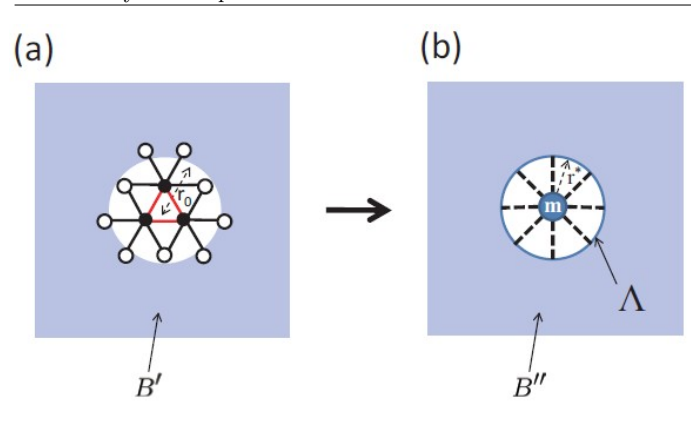


Fig. 5. Further simplification of the one-impurity Hamiltonian. Couplings between core (black) and shell (white) sites are replaced by the coupling between the impurity magnetic moment and the boundary Λ of the bulk region.

We expect the results (4.18) and (4.19) also explain the magnetic anisotropy for finite J' < 0, although the prefactors may be renormalized. In this case the magnetic moment m and the spin quadrupole moment M should be interpreted as the average among three impurity sites. This expectation is consistent with the numerical result, which will be shown in §4.5, that the anisotropy energy for finite J' < 0 as a function of J/K is qualitatively similar to those for $J' = -\infty$.

Before closing this subsection, we show for later use that it is possible to modify the single-impurity Hamiltonian (4.11) so that the exact ground state coincides with the result of the dipole approximation (4.13) and (4.17). Detailed structure of lattice part is expected to be irrelevant after the dipole approximation and we modify the Hamiltonian such that the single impurity magnetic moment interacts with a field on the boundary Λ , a circle of radius r^* , of the bulk region, as shown in Fig. 5(b). Under this simplification, the total Hamiltonian can be written as

$$H^{\pi} = H_{\text{bulk}}^{\pi} + H_{\text{imp}}^{\pi} \tag{4.21}$$

$$H_{\text{bulk}}^{\pi} = \frac{1}{2} J_{\pi} \sum_{a=1}^{3} \int_{0}^{1} d\mathbf{x} (\nabla \pi_{a})^{2}$$
 (4.22)

$$H_{\text{imp}}^{\pi} = \int_{\Lambda} d\boldsymbol{x} f\left(\boldsymbol{m}, \boldsymbol{\pi}(\boldsymbol{x})\right), \qquad (4.23)$$

where \int'' denotes the integration inside the bulk region B'' shown in Fig. 5(b). We require that the ground state of this Hamiltonian for impurity magnetic moment m is given by the result of dipole approximation (4.13) and (4.17), which we denote as $\pi_a^0(m)$.

We can uniquely determine the Hamiltonian which satisfies these conditions:

$$H^{\pi} = \frac{1}{2} J_{\pi} \sum_{a=1}^{3} \int'' d\mathbf{x} \left[\nabla \left(\pi_{a} - \pi_{a}^{0}(\mathbf{m}) \right) \right]^{2} + E_{0}^{\pi}(\mathbf{m}),$$
(4.24)

where $E_0(\mathbf{m})$ denotes the ground state energy. Clearly π_a^0 is the ground state of this Hamiltonian, and we can transform this Hamiltonian into the form of eq. (4.21)-

(4.24) by integration by parts. Therefore, we regard eq. (4.24) as the simplified single-impurity Hamiltonian. As a result, the impurity part $H_{\rm imp}^{\pi}$ is derived as

$$H_{\text{imp}}^{\pi} \equiv H^{\pi} - H_{\text{bulk}}^{\pi} = \frac{1}{2} J_{\pi} \sum_{a=1}^{3} \int_{-\infty}^{\infty} d\mathbf{x} \nabla \pi_{a}^{0}(\mathbf{m})$$

$$\cdot \left[\nabla \pi_{a}^{0}(\mathbf{m}) - 2 \nabla \pi_{a} \right] + E_{0}^{\pi}(\mathbf{m})$$

$$= -J_{\pi} \sum_{a=1}^{3} \int_{-\infty}^{\infty} d\mathbf{x} \nabla \pi_{a}^{0}(\mathbf{m}) \cdot \nabla \pi + E_{0}^{\pi}(\mathbf{m})$$

$$+ \frac{\pi J_{\pi}}{4} \left(\frac{r_{0}}{r^{*}} \right)^{2} (\mu_{0}^{\pi})^{2} (\mathbf{m}^{4} - m_{1}^{4} - m_{2}^{4} - m_{3}^{4}). \tag{4.25}$$

4.3 First Order Effect of the Interaction between the Impurity and Magnetic Excitation

Next we consider the effect of the coupling with magnetic excitation in the bulk region. Including only the first order coupling of this kind, given by eq. (4.6), the Hamiltonian for magnetic excitation becomes

$$H^{\psi} = H^{\psi}_{\text{bulk}} + H^{\psi}_{\text{imp}},$$

$$H^{\psi}_{\text{bulk}} = \frac{1}{2} J_{\psi} \sum_{a=1}^{3} \int' d\mathbf{x} \left[(\nabla \psi_{a})^{2} + k_{\psi}^{2} \psi_{a}^{2} \right], \qquad (4.26)$$

Just like the discussion above for nonmagnetic excitation, we consider only the dominant component of the magnetic excitation. The ground state configuration of ψ satisfies the Helmholtz equation $\nabla^2 \psi_a - k_{\psi}^2 \psi_a = 0$, and can be expanded in the polar coordinate as

$$\psi_a(r,\theta) = \sum_{m=0}^{\infty} c_m^{(a)} K_m(k_{\psi}r) \cos[m(\theta - \theta_{0,m}^{(a)})], \quad (4.27)$$

under the boundary condition $\psi_a(\mathbf{x}) \to 0$ with $|\mathbf{x}| \to \infty$. ¹⁸⁾ Here $K_m(x)$ denotes the modified Bessel function of the second kind. We naturally expect that the angular momentum components $c_m^{(a)}$ with large m are not dominant and neglect $c_m^{(a)}$ (m > 1). We call this "monopole-dipole approximation". We will justify this approximation by numerical calculations in §3.D. As a result, the ground state field configuration ψ is

$$\psi_a(r,\theta) = q_a^{\psi} K_0(k_{\psi}r) + K_1(k_{\psi}r) \frac{1}{r} \mathbf{r} \cdot \boldsymbol{\mu}_a^{\psi}, \qquad (4.28)$$

where we introduced a charge q_a^{ψ} and a dipole moment μ_a^{ψ} . Further, the bulk part of the energy becomes

$$E_{\text{bulk}}^{\psi} = J_{\psi} \sum_{a} \left[\left(q_{a}^{\psi} \right)^{2} \mathcal{E}_{0}(k_{\psi} r_{0}) + \left(\boldsymbol{\mu}_{a}^{\psi} \right)^{2} \mathcal{E}_{1}(k_{\psi} r_{0}) \right],$$
(4.29)

where we defined

$$\mathcal{E}_0(x) = \pi x K_0(x) K_1(x),$$

$$\mathcal{E}_1(x) = \frac{1}{2} \pi x K_0'(x) K_1'(x). \tag{4.30}$$

Now we study the ground state of the total Hamiltonian (4.26), using the monopole-dipole approximation. We deal with the ferromagnetic (J < K/2) and antiferromagnetic (J > K/2) regions separately, and first focus

on the former. Here we focus the impurity located at "E" in Fig. 4, and show the results for the other cases in Appendix A. In this case the energy of the lattice part Hamiltonian H^{ψ}_{imp} becomes

$$E_{\rm imp}^{\psi} = -\frac{\sqrt{3}}{2} J_{\psi} \sum_{a=1}^{3} \left[4 \left\{ K_0(k_{\psi} r_1) + K_1(k_{\psi} r_2) \right\} m_a q_a^{\psi} + \frac{\sqrt{3}}{3} \left\{ \frac{1}{r_1} K_1(k_{\psi} r_1) + \frac{4}{r_2} K_1(k_{\psi} r_2) \right\} m_a \hat{\kappa}'_a \cdot \mu_a^{\psi} \right],$$

$$(4.31)$$

where we defined $\hat{\kappa}'_1 = (-\sqrt{3}/2, -1/2), \hat{\kappa}'_2 = (\sqrt{3}/2, -1/2), \hat{\kappa}'_3 = (0, 1)$, and the radial coordinates of shell sites $r_1 = \sqrt{21}/3$ and $r_2 = 2\sqrt{3}/3$. The total energy is the sum of the bulk part (4.29) and the impurity part (4.31), and given by

$$E = J_{\psi} \sum_{a} \left[\mathcal{E}_{0}(k_{\psi}r_{0}) \left\{ (q_{a}^{\psi} - q_{0}^{\psi}m_{a})^{2} - (q_{0}^{\psi})^{2}m_{a}^{2} \right\} + \mathcal{E}_{1}(k_{\psi}r_{0}) \sum_{a} \left\{ (\boldsymbol{\mu}_{a}^{\psi} - \mu_{0}^{\psi}m_{a}\hat{\boldsymbol{\kappa}}_{a}')^{2} - (\mu_{0}^{\psi})^{2}m_{a}^{2} \right\} \right],$$

$$(4.32)$$

where we defined

$$q_0^{\psi} = \frac{\sqrt{3}}{\mathcal{E}_0(k_{\psi}r_0)} \left(K_0(k_{\psi}r_1) + K_0(k_{\psi}r_2) \right) \tag{4.33}$$

$$\mu_0^{\psi} = \frac{1}{4\mathcal{E}_1(k_{\psi}r_0)} \left(\frac{1}{r_1} K_1(k_{\psi}r_1) + \frac{4}{r_2} K_1(k_{\psi}r_2) \right). \tag{4.34}$$

Therefore, the charge and the dipole moment are determined by minimizing this energy as

$$q_a^{\psi} = q_0^{\psi} m_a, \quad \boldsymbol{\mu}_a^{\psi} = \mu_0^{\psi} m_a \hat{\boldsymbol{\kappa}}_a',$$
 (4.35)

and the ground state energy is

$$E_0^{\psi}(\boldsymbol{m}) = -J_{\psi} \left[\mathcal{E}_0(k_{\psi}r_0) \left(q_0^{\psi} \right)^2 + \mathcal{E}_1(k_{\psi}r_0) \left(\mu_0^{\psi} \right)^2 \right]$$

$$(4.36)$$

Note that this ground state energy does not depend on the direction of the impurity magnetic moment m. It means that magnetic excitation does not contribute to the anisotropy energy of the impurity magnetic moment, in the first order coupling discussed here.

Next we turn to the antiferromagnetic region (J > K/2). The lattice part of the energy becomes

$$E_{\text{imp}}^{\psi} = -\frac{\sqrt{3}}{2} J_{\psi} \sum_{a=1}^{3} \left(\frac{1}{r_{1}} K_{1}(k_{\psi} r_{1}) + \frac{4}{r_{2}} K_{1}(k_{\psi} r_{2}) \right) m_{a} \hat{\kappa}_{a} \cdot \mu_{a}^{\psi}. \tag{4.37}$$

Combining this with the bulk part (4.30) yields the total energy

$$E = J_{\psi} \sum_{a} \left[\mathcal{E}_{0}(k_{\psi}r_{0}) \left(q_{a}^{\psi}\right)^{2} + \mathcal{E}_{1}(k_{\psi}r_{0}) \right]$$

$$\times \left\{ \left(\boldsymbol{\mu}_{a}^{\psi} - \tilde{\mu}_{0}^{\psi} m_{a} \hat{\boldsymbol{\kappa}}_{a}\right)^{2} - \left(\tilde{\mu}_{0}^{\psi}\right)^{2} m_{a}^{2} \right\} , \qquad (4.38)$$

where we defined $\tilde{\mu}_0^{\psi} = \sqrt{3}\mu_0^{\psi}$. Therefore, the charge and

the dipole moment are given by

$$q_a^{\psi} = 0, \quad \boldsymbol{\mu}_a^{\psi} = \tilde{\mu}_0^{\psi} m_a \hat{\boldsymbol{\kappa}}_a, \tag{4.39}$$

and the ground state energy is

$$E_0^{\psi}(\boldsymbol{m}) = -J_{\psi} \mathcal{E}_1(k_{\psi} r_0) \left(\tilde{\mu}_0^{\psi}\right)^2. \tag{4.40}$$

Note that this energy does not depend on the direction of impurity magnetic moment m, just as in the ferromagnetic region. It is notable that the first order effect of magnetic excitation in the bulk region does not yield the anisotropy of impurity magnetic moment in either ferromagnetic or antiferromagnetic region. We will see in the next subsection, however, magnetic excitation does contribute to the anisotropy energy through second order coupling.

Just like in the previous subsection, we can modify the single-impurity Hamiltonian (4.26) so that the monopole-dipole approximation is exact:

$$H^{\psi} = \frac{1}{2} J_{\psi} \sum_{a=1}^{3} \int_{-\infty}^{\infty} d\boldsymbol{x} \left\{ \left[\nabla (\psi_{a} - \psi_{a}^{0}(\boldsymbol{m})) \right]^{2} + k_{\psi}^{2} \left[\psi_{a} - \psi_{a}^{0}(\boldsymbol{m}) \right]^{2} \right\} + E_{0}^{\psi}(\boldsymbol{m}), \qquad (4.41)$$

where ψ_a^0 denotes the field configuration of the ground state in monopole-dipole approximation. The impurity part H_{imp}^{ψ} is derived as

$$H_{\text{imp}}^{\psi} = \frac{1}{2} J_{\psi} \sum_{a=1}^{3} \int_{-\infty}^{\infty} d\mathbf{x} \left\{ \nabla \psi_{a}^{0} \cdot \left[\nabla \psi_{a}^{0} - 2 \nabla \psi_{a} \right] + k_{\psi}^{2} \psi_{a}^{0} \left[\psi_{a}^{0} - 2 \psi_{a} \right] \right\} + E_{0}^{\psi}(\mathbf{m})$$

$$= -J_{\psi} \sum_{a=1}^{3} \int_{-\infty}^{\infty} d\mathbf{x} \left[\nabla \psi_{a}^{0} \cdot \nabla \psi_{a} + k_{\psi}^{2} \psi_{a}^{0} \psi_{a} \right] + E_{0}^{\psi}(\mathbf{m})$$

$$+ J_{\psi} \sum_{a=1}^{3} \left[\left(q_{a}^{\psi} \right)^{2} \mathcal{E}_{0}(k_{\psi} r^{*}) + \left(\boldsymbol{\mu}_{a}^{\psi} \right) \mathcal{E}_{1}(k_{\psi} r^{*}) \right].$$

$$(4.42)$$

Finally let us calculate the total induced magnetic moments $\delta \boldsymbol{m} \equiv \sum_{i \notin \text{core}} \langle \boldsymbol{S} \rangle$, and the total squared induced magnetic moments $\delta m_{\text{sq}}^2 \equiv \sum_{i \notin \text{core}} \langle \boldsymbol{S} \rangle^2$. In the ferromagentic region, these are derived by using magnetic excitation $\boldsymbol{\psi}$ as

$$\delta \boldsymbol{m} = \frac{8}{3\sqrt{3}} \int'' d\boldsymbol{r} \boldsymbol{\psi} = \frac{16\pi}{3\sqrt{3}} q_0^{\psi} \boldsymbol{m} \frac{r_0}{k_{\psi}} K_1(k_{\psi} r_0) \quad (4.43)$$

$$\delta m_{\text{sq}}^2 = \frac{8}{3\sqrt{3}} \int'' d\boldsymbol{r} \boldsymbol{\psi}^2$$

$$= \frac{8}{3\sqrt{3}} \pi r_0^2 \left\{ (q_0^{\psi})^2 \left[K_1^2(k_{\psi} r_0) - K_0^2(k_{\psi} r_0) \right] + \frac{1}{2} (\mu_0^{\psi})^2 \left[K_0^2(k_{\psi} r_0) - K_1^2(k_{\psi} r_0) - \frac{2}{k_{\psi} r_0} K_0(k_{\psi} r_0) K_1(k_{\psi} r_0) \right] \right\} \quad (4.44)$$

These values diverge as 1/J for $J \to 0$. Note that this divergence should not be literally taken. For small J, magnetic excitation ψ on the sites near the impu-

rity are not negligible and perturbative approach with regard to ψ breaks down. Therefore we anticipate actual divergence of induced magnetic moment δm is weaker than 1/J. In the antiferromagnetic region, the present approach does not predict the value of the total induced magnetic moment δm , since the field variable ψ corresponds to the staggered magnetization. On the other hand, total squared moments $m_{\rm sq}$ can still be represented by the first line of eq. (4.44) and we obtain

$$\delta m_{\rm sq}^2 = \frac{4}{3\sqrt{3}} \pi r_0^2 (\tilde{\mu}_0^{\psi})^2 \left[K_0^2 (k_{\psi} r_0) - K_1^2 (k_{\psi} r_0) - \frac{2}{k_{\psi} r_0} K_0 (k_{\psi} r_0) K_1 (k_{\psi} r_0) \right], \tag{4.45}$$

which diverges as 1/(1-K/J) for $J\to K$. Again, actual divergence is expected to be weaker. We will numerically investigate these two representations of induced magnetic moment in §4.6.

4.4 Second Order Effect of the Interaction between the Impurity and Bulk Excitation

In the previous argument, we showed that the magnetic anisotropy emerges from the first order coupling to nonmagnetic excitation in the bulk region, and that the anisotropy is corner-cubic one represented by eq. (4.18). We will confirm this, by means of numerical calculations in the next subsection, but we will also find different types of anisotropy appear when J/K is small. They originate from higher-order effects of the coupling between impurity magnetic moment and bulk excitations. In this subsection we examine the effects of the second order coupling and investigate the magnetic anisotropy. Adding the three second-order terms (4.7)-(4.9), the total Hamiltonian is now given by

$$H^{(2)} = H_{\text{bulk}}^{\pi} + H_{\text{bulk}}^{\psi} + H_{\text{imp}}^{\pi} + H_{\text{imp}}^{\psi} + H_{\text{imp}}^{\pi^{2}} + H_{\text{imp}}^{\psi^{2}} + H_{\text{imp}}^{\pi\psi}$$
(4.46)

where the bulk parts H_{bulk}^{π} and H_{bulk}^{ψ} are given in eq. (4.11) and (4.26), respectively. As for the bulk region, we have employed the dipole approximation for the nonmagnetic excitation π , and the monopole-dipole approximation for the magnetic excitation ψ . Here we introduce two additional approximations, in order to simplify the problem. First, we consider only the lowest-order nonzero angular momentum component for the magnetic excitation ψ . As is clear from the previous results (4.35) and (4.39), it corresponds to the monopole approximation for the ferromagnetic region (J < K/2) and dipole approximation for the antiferromagnetic region (J > K/2). Numerical calculations in the next subsection shows that these lowest-order moments are more than several times larger than the higher order moments. Second, we assume that the dipole moments for the field variables point to the direction obtained in the first order calculation. Again, numerical calculations will verify this approximation. As a result of these two approximations, the field variables are represented as

$$\pi_a(\mathbf{r}) = \frac{r_0}{r^2} \mu_a^{\pi} \hat{\mathbf{k}}_a \cdot \mathbf{r},\tag{4.47}$$

$$\psi_a(\mathbf{r}) = q_a^{\psi} K_0(k_{\psi}r) \qquad F.M. \tag{4.48}$$

$$\psi_a(\mathbf{r}) = K_1(k_{\psi}r) \frac{1}{r} \mu_a^{\pi} \cdot \hat{\mathbf{k}}_a \cdot \mathbf{r} \qquad A.F.M., \tag{4.49}$$

with scalar variables μ_a^{π}, q_a^{ψ} , and μ_a^{ψ} . Note that it is straightforward, though not shown here, to extend the following argument to more general situation that we do not employ these approximations.

Now let us calculate the ground state energy of the Hamiltonian (4.46) within the approximations above, and we first focus on the ferromagnetic region (J < K/2). For the configuration (4.47)-(4.49), the energy becomes

$$E^{(2)} = \sum_{I,J=\pi,\psi} \mathbf{g}_I \cdot \hat{M}_{IJ} \mathbf{g}_J - 2 \sum_{I=\pi,\psi} \mathbf{f}_I \cdot \mathbf{g}_I \qquad (4.50)$$

where f_I and g_I , $(I = \pi, \psi)$ are three-component vectors

$$\mathbf{f}_{\pi} = c_{\pi} \mu_0^{\pi} \left(m_2 m_3, m_3 m_1, m_1 m_2 \right)^T \tag{4.51}$$

$$\mathbf{f}_{\psi} = c_{\psi} q_0^{\psi} \left(m_1, m_2, m_3 \right)^T \tag{4.52}$$

$$\boldsymbol{g}_{\pi} = (\mu_1^{\pi}, \mu_2^{\pi}, \mu_3^{\pi})^T \tag{4.53}$$

$$\mathbf{g}_{\psi} = \left(q_1^{\psi}, q_2^{\psi}, q_3^{\psi}\right)^T, \tag{4.54}$$

 \hat{M}_{IJ} 's are three-by-three matrices

$$(M_{\pi\pi})_{ij} = c_{\pi}\delta_{ij} + \frac{1}{2}c_{\pi^2}(1 - \delta_{ij})m_i m_j,$$

$$(M_{\psi\psi})_{ij} = c_{\psi}\delta_{ij} + \frac{1}{2}c_{\psi^2}(1 - \delta_{ij})m_i m_j,$$

$$(M_{\pi\psi})_{ij} = (M_{\psi\pi})_{ij} = \frac{1}{4}c_{\pi\psi}\sum_{k=1}^{3} |\epsilon_{ijk}| m_k,$$
 (4.55)

with coefficients

$$c_{\pi} = \frac{\pi J_{\pi}}{2} r_0^2, \ c_{\psi} = J_{\psi} \mathcal{E}_0 \left(k^{\psi} r_0 \right), \ c_{\pi^2} = -\frac{369}{98} K r_0^2,$$

$$(4.56)$$

$$c_{\psi^2} = 2K \left\{ K_0 \left(k_{\psi} r_1 \right)^2 + K_0 \left(k_{\psi} r_2 \right)^2 \right\}$$
 (4.57)

$$c_{\pi\psi} = -2(2J - K)r_0 \left\{ \frac{1}{2r_1^2} K_0 \left(k_{\psi} r_1 \right) + \frac{2}{r_2^2} K_0 \left(k_{\psi} r_2 \right) \right\}$$
(4.58)

The ground state energy of the Hamiltonian (4.50) is readily derived as

$$E_0(\boldsymbol{m}) = -\sum_{I,J=\pi,\psi} \boldsymbol{f}_I \cdot (\hat{M}_{IJ} - \hat{\Sigma}_{IJ})^{-1} \boldsymbol{f}_J \qquad (4.59)$$

Here, the self-energy part is given as

$$\hat{\Sigma}_{\pi\pi} = \hat{M}_{\pi\psi} \hat{M}_{\psi\psi}^{-1} \hat{M}_{\psi\pi}, \quad \hat{\Sigma}_{\psi\psi} = \hat{M}_{\psi\pi} \hat{M}_{\pi\pi}^{-1} \hat{M}_{\pi\psi} \quad (4.60)$$

$$\hat{\Sigma}_{\pi\psi} = \hat{M}_{\psi\psi} \hat{M}_{\psi\pi}^{-1} \hat{M}_{\pi\pi}, \quad \hat{\Sigma}_{\psi\pi} = \hat{M}_{\pi\pi} \hat{M}_{\pi\psi}^{-1} \hat{M}_{\psi\psi} \quad (4.61)$$

and represents the effects of coupling between nonmagnetic and magnetic excitations. (We do not show the explicit form of the ground state energy, since it is quite lengthy.) Later we investigate the dependency of the ground state energy on the coupling constants J/K.

Next, we turn to the antiferromagnetic region (J > K/2). The ground state energy is similarly calculated

and the result is given by replacing the variables in eqs. (4.59)-(4.61) by those for the antiferromagnetic region as

$$c_{\psi^2} = -K \left[\left(\frac{1}{r_1} K_1(k_{\psi}) \right)^2 - 2 \left(\frac{1}{r_2} K_1(k_{\psi} r_2) \right)^2 \right]$$
(4.62)

$$c_{\pi\psi} = 2(2J - K)r_0 \left[-\frac{13}{4r_1^3} K_1(k_{\psi}r_1) + \frac{2}{r_2^3} K_1(k_{\psi}r_2) \right]$$
(4.63)

$$c_{\psi} = J_{\psi} \mathcal{E}_1(k_{\psi} r_0). \tag{4.64}$$

and q_0^ψ in eq. (4.52) and q_a^ψ (a=1,2,3) in eq. (4.54) should be replaced with $\tilde{\mu}_0^\psi$ and μ_a^ψ ,respectively.

We show later in Fig. 8 (b) the ground state energy (4.59) as a function of J/K when the impurity magnetic moment is fixed along the representative directions. We can see that the energy now depends on J/K, unlike the results with the first order coupling (4.18) and (4.36). This is an effect of the second-order couplings c_{π^2} , c_{ψ^2} and $c_{\pi\psi}$. In the parameter region 0 < J/K < 0.077, (100) direction is an easy direction, i.e. the anisotropy is "face-cubic". We will compare this result with numerical results in the next subsection.

4.5 Numerical Calculation

We have shown analytically the appearance of the magnetic anisotropy and the configuration of the ground state, based on the effective field theory for the low-energy excitations in the bulk region. In this subsection we numerically solve this one impurity problem, in order to compare with the approximate analytical results in the previous subsections.

We calculated the ground-state energy and spin configuration, by numerical calculations with finite-size clusters up to L=40, including 5292 sites. The geometry of the cluster is depicted in Fig. 6. L labels the layer of sites away from the impurity bond triad placed at the origin, and it characterizes the cluster size. To minimize finite-size effects, we set the spin wavefunctions on the outer-boundary sites (shown by black circles in Fig. 6) to the bulk values (1.2). With this boundary condition, we minimize the energy (3.4) by optimizing wavefunctions of each spin. As for the ferromagnetic coupling between core sites J' < 0, we examined both of finite and infi-

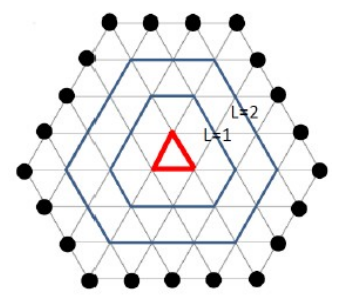
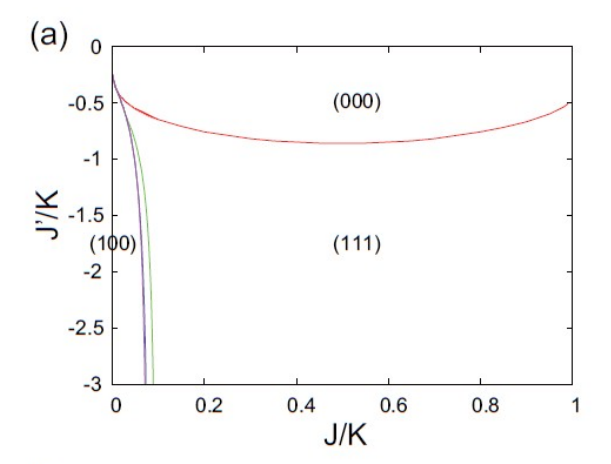


Fig. 6. The geometry of the finite size sample used in the numerical calculation. The case of size L=2 is shown. States on the sites denoted by black circles are fixed to the mean-field ground state (1.2).

nite case. For the infinite case $(J' = -\infty)$, we fixed the direction of impurity magnetic moment and examined the ground state for each value of the impurity magnetic moment, in order to compare with the analytical results.

First let us show the results for finite J'. Fig. 7 shows the phase diagram and each phase is characterized by the easy directions of the average magnetic moment of the three core sites: $\overline{m} \equiv \frac{1}{3} \sum_{i \in \text{core}} m_i$. We find that there are five phases with different easy axes and label these phases as shown in Table I. The (111) phase has a corner-cubic anisotropy, and covers the largest region of the coupling J/K, when |J'| is sufficiently large. On the other hand, the (100) phase has a face-cubic anisotropy and appears near the J=0 line. Moreover, between these two phases we find the (110) phase, which has an edge-cubic anisotropy, and the least symmetric (ab0) phase.



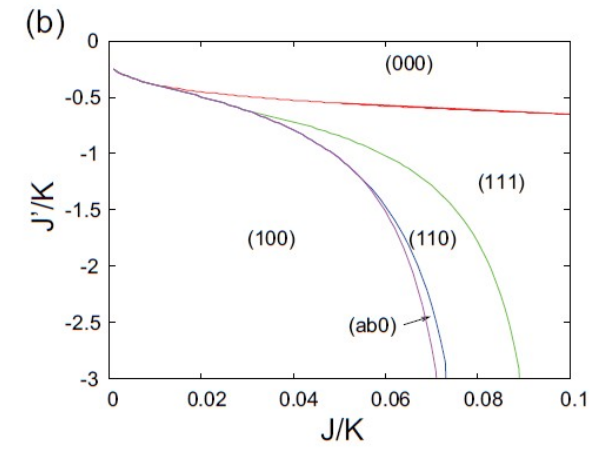


Fig. 7. Phase diagram of the ground state in J-J' parameter space. (a) $0 \le J/K \le 1$, (b) $0 \le J/K \le 0.1$.

Table I. Labeling of five phases and easy directions of impurity magnetic moment in each phase.

| label | easy directions | | | |
|-------|---|--|--|--|
| (000) | (0,0,0) | | | |
| (111) | $\frac{1}{\sqrt{3}}(\pm 1, \pm 1, \pm 1)$ | | | |
| (110) | $\frac{1}{\sqrt{2}}(\pm 1, \pm 1, 0), \frac{1}{\sqrt{2}}(\pm 1, 0, \pm 1), \frac{1}{\sqrt{2}}(0, \pm 1, \pm 1)$ | | | |
| (ab0) | $(\pm a, \pm b, 0), (\pm b, \pm a, 0), (\pm a, 0, \pm b), (\pm b, 0, \pm a), (0, \pm a, \pm b), (0, \pm b, \pm a) (a^2 + b^2 = 1)$ | | | |
| (100) | $(\pm 1, 0, 0), (0, \pm 1, 0), (0, 0, \pm 1)$ | | | |

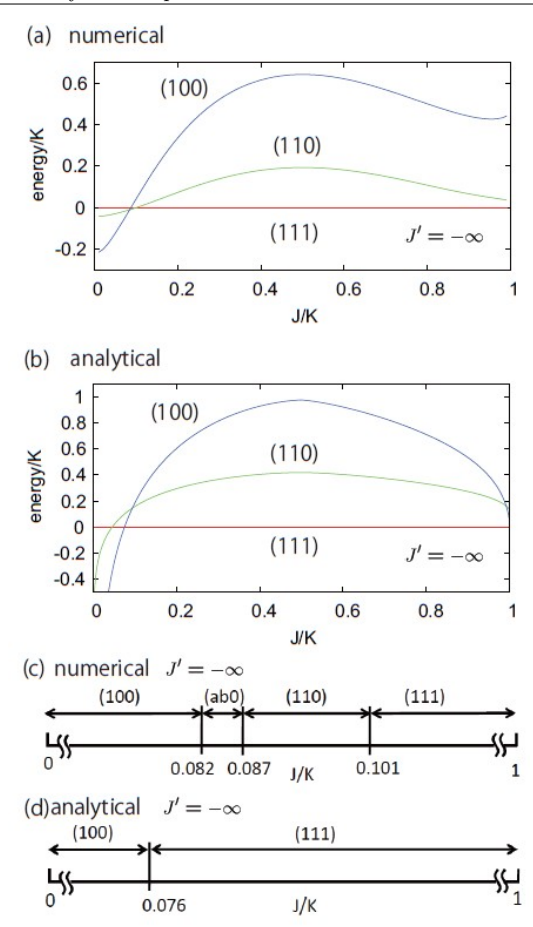


Fig. 8. (a)(b)Energies of the (111) and (110) states measured from the energy of the (100) state in the limit $J' = -\infty$. (a):numerical result, (b):analytical result. (c)(d) The ground state phase diagram in the limit $J' = -\infty$. (c):numerical result, (d):analytical result.

Second we show the results in the limit $J' = -\infty$. Fig. 8(a) and (c) show the energy difference between three representative phases and the phase diagram, respectively. The corresponding analytical results are shown in Fig. 8(b) and (d). The four phases observed at finite |J'|, survive in this $J' = -\infty$ limit, as shown in Fig. 8 (c). It implies that the finiteness of |J'| is not essential for the presence of these anisotropies of the impurity magnetic moment. Further, the appearance of the two phases (100) and (111), which cover large regions in the phase diagram, qualitatively agrees with the analytical results shown in Fig. 8 (d), whereas the other two phases appear only in numerical calculation. The dependency of the magnetic anisotropy energy, shown in Fig. 8(a), qualitatively agrees with the analytical results in Fig. 8(b), although the difference becomes significant near J/K = 0 or 1. This discrepancy can possibly be ascribed to the breakdown of the perturbative treatment of the magnetic excitation. Near the onset of magnetically ordered phases (J/K = 0 or 1), the system becomes sensitive to the magnetic impurity and the amplitude of the field for magnetic excitation increases.

Then we examine the ground state spin configuration $\langle S_i \rangle$ in the limit $J' = -\infty$. As a typical example, we fix the impurity magnetic moment as $m = \frac{1}{\sqrt{3}}(1,1,1)$. Be-

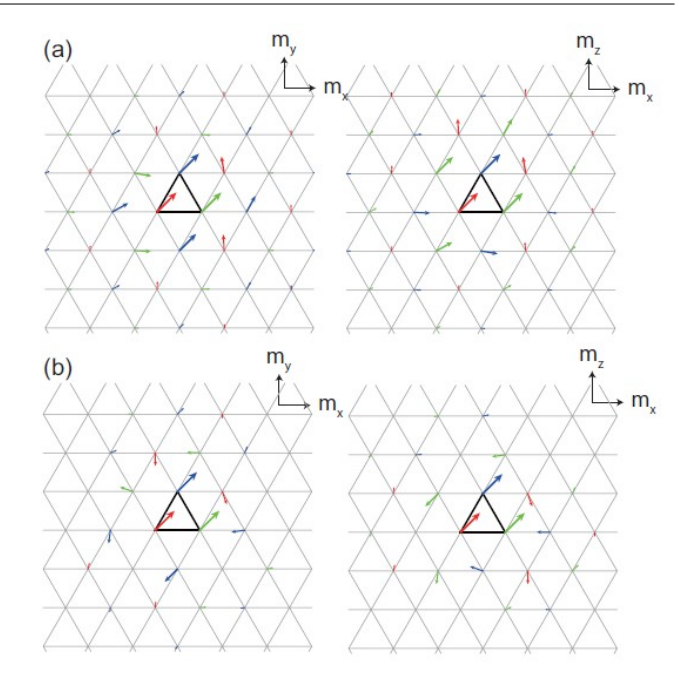


Fig. 9. Numerical result of spatial distribution of induced magnetic moments in the limit $J' = -\infty$ and $m = \frac{1}{\sqrt{3}}(1, 1, 1)$. (a) ferromagnetic case (J/K = 0.05), (b) antiferromagnetic case (J/K = 0.95). Projections to XY and XZ planes are shown in the left and right panel, respectively.

fore detailed argument, we show induced magnetic moments around the impurity in the ferromagnetic region (J/K=0.05) in Fig. 9 (a), and in the antiferromagnetic region (J/K=0.95) in (b). In both regions, induced magnetic moments form a complex noncoplanar pattern. This noncoplanarity can be understood as the result of antiferro quadrupolar order. As mentioned in §3.2, magnetic moments are perpendicular to the directors, which are orthogonal between different sublattices. Note that this orthogonality is violated around the impurity, due to the nonmagnetic excitation.

In order to compare the results with analytical ones, we converted the spin configuration to the field variables for nonmagnetic and magnetic excitation, by solving equations (4.2) and (4.3). The results are shown in Fig. 10. Nonmagnetic excitation π_1 around the impurity is plotted for two-dimensional space in Fig. 10(a) and also along one direction in Fig. 10(b). We can see that it shows dipole-like angle dependence, changing sign once around the impurity site, and its radial dependence decays as 1/r. This result verifies the dipole approximation employed in §4.2 at least on the qualitative level. The direction of the principal axis is $\hat{\kappa}_1 = (1/2, -\sqrt{3}/2)$ and coincides with that in the analytical result (4.17). Next we turn to the magnetic excitation ψ , and show it in Fig. 10 (c) and (d) for the ferromagnetic region (J/K = 0.1) and Fig. 10 (e)(f) for the antiferromagnetic region (J/K = 0.9). Its angular part has isotropic (dipole-like) in the ferromagnetic (antiferromagnetic) region, and the radial dependence decays exponentially in both cases. These results verify the monopole-dipole approximation we used in §4.1. Again, for the antiferromagnetic region, the direction of the principal axis is $\hat{\kappa}_1$ and

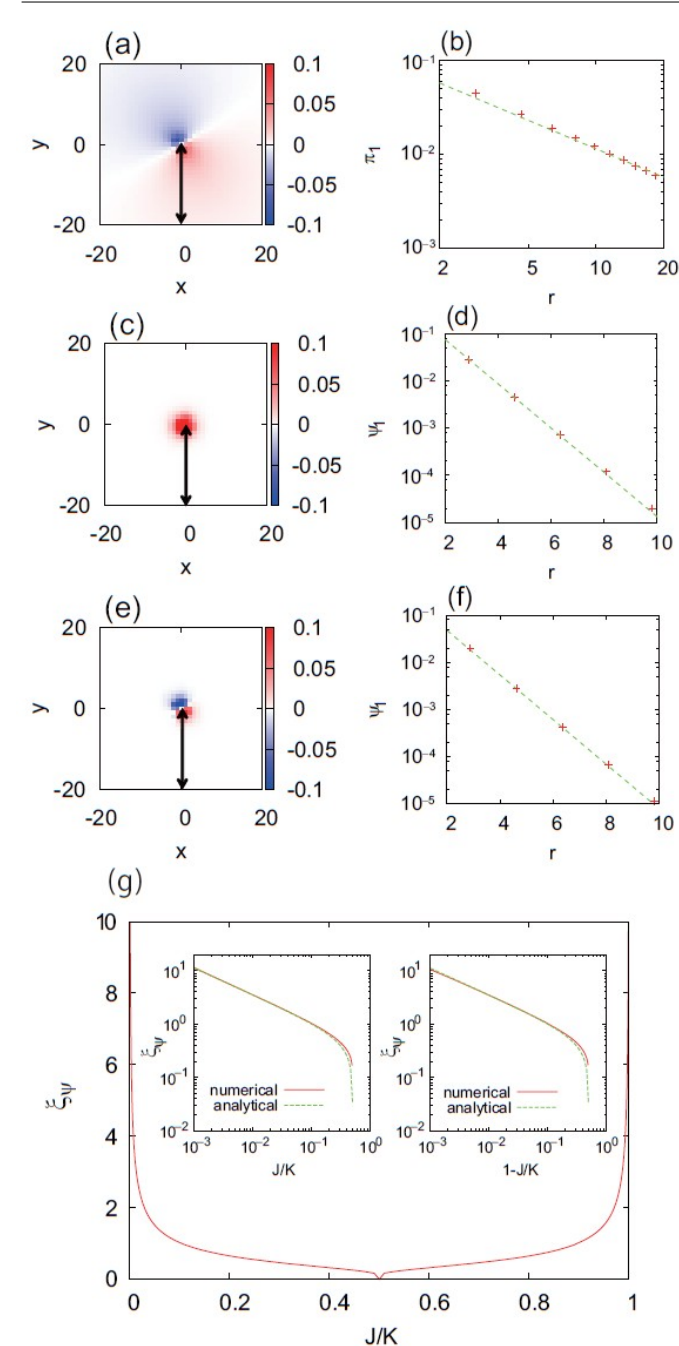


Fig. 10. Numerical results of spatial distribution of the field variables for $J'=-\infty$ and $\boldsymbol{m}=\frac{1}{\sqrt{3}}(1,1,1)$. (a):Nonmagnetic excitation π_1 for J/K=0.5. (b):Log-log plot of π_1 along the arrow in (a). (c):Magnetic excitation ψ_1 for J/K=0.1. (d):Semilog plot of ψ_1 along the arrow in (c). (e): ψ_1 for J/K=0.9. (f):Semilog plot of ψ_1 along the arrow in (e). (g):Decay length of ψ_1 . Two insets show log-log plots of $\xi_{\psi}=1/k_{\psi}$ near J/K=0 and 1, together with analytical prediction (3.20).

agrees with that in the analytical result (4.39). In Fig. 10(g) we present the decay length ξ_{ψ} of magnetic excitation ψ , which is derived by fitting the radial dependence of ψ to the exponential form $\psi(r) \propto \exp(-r/\xi_{\psi})$. In the regions near the phase boundary with ferromagnetic (antiferromagnetic) phase, 0 < J/K < 0.1 (0.9 < J/K < 1), ξ_{ψ} agrees well with its analytical value $\xi_{\psi} = 1/k_{\psi}$. In the intermediate region 0.1 < J/K < 0.9 with $\xi_{\psi} \lesssim 1$, on the other hand, there exist discrepancy between numeri-

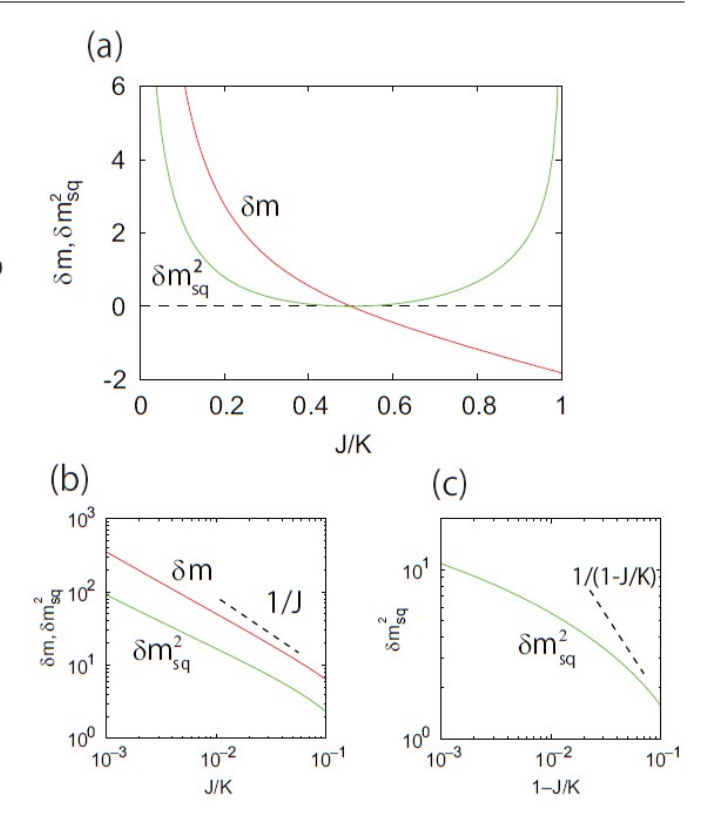


Fig. 11. (a): Induced magnetic moment δm measured along the direction of impurity magnetic moment $\delta m = m \cdot \delta m$ and total squared induced moment $\delta m_{\rm sq}^2$, in the limit $J' = -\infty$ and $m = \frac{1}{\sqrt{3}}(1,1,1)$. (b): Log-log plot in the ferromagnetic region. (c): Log-log plot in the antiferromagnetic region. Notice the horizontal axis is 1 - J/K. Cluster size is carefully chosen so that the finite size effect is negligible (less than 1%).

cal and analytical values. This discrepancy is ascribed to the coarse graining of the lattice model, which is justified only when the characteristic length scale ξ_{ψ} of the theory is much larger than the lattice constant.

In order to further examine the validity of the simplification of the angular part for π and ψ , we calculated the amplitude of each partial wave in eqs. (4.12) and (4.27) up to quadrupole (m=2) component. The results are listed in Table II. We can see that the dominant component (i.e. ($\mu^{\pi}(J=0.1,0.5,0.9),\ q^{\psi}(J=0.1),\ \mu^{\psi}(J=0.9)$) is more than several times larger than the other components. This justifies our approximation that only single dominant component is taken into account.

Finally let us examine induced magnetic moments outside the impurity δm . Fig. 11 shows total induced mag-

Table II. Angular momentum components of the field variables for $\mathbf{m} = \frac{1}{\sqrt{3}}(1,1,1)$. q,μ , and d denote the absolute values of monopole, dipole, and quadrupole component respectively.

| | | J/K | | |
|--------|--------------|-------|-------|-------|
| | | 0.1 | 0.5 | 0.9 |
| π | μ^{π} | 0.086 | 0.138 | 0.125 |
| | d^{π} | 0.013 | 0.003 | 0.029 |
| ψ | q^{ψ} | 0.529 | - | 0.000 |
| | μ^{ψ} | 0.113 | - | 0.925 |
| | d^{ψ} | 0.028 | - | 0.207 |

netic moment $\delta \boldsymbol{m}$ and total squared induced magnetic moment $\delta m_{\rm sq}^2$, defined in §4.3, as functions of J/K for (111) phase. In the ferromagnetic region, $\delta \boldsymbol{m}$ is parallel to the impurity magnetic moment and $\delta \boldsymbol{m}$ and $\delta m_{\rm sq}^2$ diverge with $J \to 0$. This divergence is slightly weaker than 1/J, as mentioned in §4.3. In the antiferromagnetic region, is antiparallel to the impurity magnetic moment, as anticipated from antiferromagnetic interaction. Contrary to the ferromagnetic region, the absolute value of induced magnetic moment remains finite as $J \to K$. The squared moment $m_{\rm sq}$ diverges with $J/K \to 1$ and the divergence is weaker than analytically derived behavior, $(1-J/K)^{-1}$.

5. Interaction between Impurities

In the previous section, we showed that magnetic and nonmagnetic excitations are induced around an impurity magnetic moment. When there exist multiple impurities, interference of these excitations causes interaction between impurities. In this section, we study this impurity-impurity interaction, using both analytical and numerical methods. We will show that nonmagnetic excitation yields long-range interaction with spatial anisotropy.

In order to derive interaction between impurities, let us consider a system with two impurities with their magnetic moments fixed, and calculate its ground state energy. As in the previous section, we describe the bulk part by the continuum effective model, as shown in Fig. 5. Regarding the impurity part $H_{\rm imp}$, we consider only the first order coupling of impurity magnetic moment and bulk excitations. As a result we can decompose the Hamiltonian in the magnetic and nonmagnetic parts as $H = H^{\pi}(\{\pi\}) + H^{\psi}(\{\psi\})$, and study the ground state of each part separately, just like the discussion in the previous section.

For each single impurity, we take only the most dominant angular component of excitations, π and ψ , in the bulk region. It corresponds to the dipole approximation for the nonmagnetic excitation π . As for the magnetic excitation ψ , the dominant mode is a dipole component in the antiferromagnetic region (J/K>2), and a scalar component in the ferromagnetic region (J<K/2). We use the minimal models of impurity (4.24) and (4.41), for which these approximations are exact. In these models, we take the limit $r^* \to 0$, where r^* denotes the radius of the void of the bulk region shown in Fig. 5(b), since finiteness of r^* is irrelevant to the asymptotic behavior of the interaction energy as the separation tends to infinity.

We will analytically derive the interaction mediated by nonmagnetic and magnetic excitations in §5.1 and §5.2, respectively, and then proceed to numerical analysis in §5.3.

5.1 Interaction Mediated by Nonmagnetic Excitation

Let us derive the interaction energy between two impurities mediated by nonmagnetic excitation in the bulk. Using the simplified one-impurity Hamiltonian (4.21), (4.22) and (4.25), the total Hamiltonian with two impurities is given by

$$H^\pi = \!\! H_{\mathrm{bulk}}^\pi + H_{\mathrm{imp}}^{\pi(a)} + H_{\mathrm{imp}}^{\pi(b)}$$

$$= \frac{1}{2} J_{\pi} \int d\boldsymbol{x} \left\{ \nabla \left(\boldsymbol{\pi} - \left(\boldsymbol{\pi}^{0(\alpha)} + \boldsymbol{\pi}^{0(\beta)} \right) \right) \right\}^{2}$$
$$- J_{\pi} \int d\boldsymbol{x} \nabla \boldsymbol{\pi}^{0(\alpha)} \cdot \nabla \boldsymbol{\pi}^{0(\beta)}$$
$$+ E_{0}(\boldsymbol{m}^{(\alpha)}) + E_{0}(\boldsymbol{m}^{(\beta)}), \tag{5.1}$$

where $\boldsymbol{m}^{(i)}$ and $\boldsymbol{\pi}^{0(i)}$, $(i=\alpha,\beta)$ denote the impurity magnetic moments and the ground state configuration in the presence of the individual impurity, respectively. $i=\alpha,\beta$ denotes the impurity index. Note that $\boldsymbol{\pi}^0$ itself depends on the magnetic moment at the impurity, $\boldsymbol{\pi}^{0(i)}=\boldsymbol{\pi}^0(\boldsymbol{x};\boldsymbol{m}^{(i)})$. We can define the interaction energy H_{int}^{π} as the difference between the ground state energy of the whole system, which is calculated for eq. (5.1), and the sum of the two ground state energies of the one-impurity Hamiltonians:

$$H_{\text{int}}^{\pi} \equiv E_{\text{g.s.}} - \left(E_0(\boldsymbol{m}^{(\alpha)}) + E_0(\boldsymbol{m}^{(\beta)}) \right)$$
$$= -J_{\pi} \int d^2x \nabla \boldsymbol{\pi}^{0(\alpha)} \cdot \nabla \boldsymbol{\pi}^{0(\beta)}$$
(5.2)

Using the expression of the one-impurity ground state (4.13) and (4.17), the interaction energy is expressed in terms of three-by-three matrices

$$H_{\text{int}}^{\pi} = \pi J_{\pi} \frac{r_0^2 (\mu_0^{\pi})^2}{r_{\alpha\beta}^2} \text{Tr} \left(T^{(\alpha)} f T^{(\beta)} \right)$$
 (5.3)

$$\left(T^{(x)}\right)_{ab} = m_a^{(x)} m_b^{(x)} - \delta_{ab} m_a^{(x)^2}, \quad (x = \alpha, \beta)$$
 (5.4)

$$f = \begin{pmatrix} \cos(2\theta + \frac{2\pi}{3}) & 0 & 0\\ 0 & \cos(2\theta - \frac{2\pi}{3}) & 0\\ 0 & 0 & \cos 2\theta \end{pmatrix},$$
(5.5)

where the separation between the two impurities is expressed as $\mathbf{r}_{\beta} - \mathbf{r}_{\alpha} \equiv \mathbf{r}_{\alpha\beta} = r_{\alpha\beta}(\cos\theta,\sin\theta)$. The interaction is biquadratic with regard to impurity magnetic moments \mathbf{m} , and its radial part has r^{-2} dependence, whereas its angular part has dipole-dipole like anisotropy. Note that nonzero elements of T matrix are nothing but t_{2g} part of spin quadrupole moment defined by eq. (4.20). Therefore the interaction (5.3) can also be interpreted as interaction between quadrupole moments of impurity spins.

5.2 Interaction Mediated by Magnetic Excitation

Second let us derive the interaction between impurities mediated by magnetic excitations, using simplified one-impurity Hamiltonian (4.41). The result is different between the ferromagnetic and antiferromagnetic regions $(J \geq K/2)$.

In the ferromagnetic region (J < K/2), the interaction energy is

$$H_{\rm int}^{\psi} = -2\pi J_{\psi}(q_0^{\psi})^2 K_0(k_{\psi}r_{\alpha\beta}) \boldsymbol{m}^{(\alpha)} \cdot \boldsymbol{m}^{(\beta)}, \qquad (5.6)$$

where $K_0(x)$ denotes the modified Bessel function of the second kind. The long-range asymptotic form is given by

$$H_{\rm int}^{\psi} \sim -\sqrt{\frac{2\pi^3}{k_{\psi}r_{\alpha\beta}}}J_{\psi}(q_0^{\psi})^2 e^{-k_{\psi}r_{\alpha\beta}}\boldsymbol{m}^{(\alpha)}\cdot\boldsymbol{m}^{(\beta)}, \quad (5.7)$$

where we used the asymptotic form of the modified Bessel function of the second kind $K_{\nu}(z)$ as $z \to \infty$:

$$K_{\nu}(z) = \sqrt{\frac{\pi}{2z}}e^{-z}\left[1 + \frac{4\nu^2 - 1}{8z} + \cdots\right]$$
 (5.8)

The expression (5.7) shows that the interaction is ferromagnetic and isotropic in both of the spin space and the real space, and exponentially decays with the characteristic length scale of magnetic excitation,

$$\frac{1}{k_{\psi}} = \frac{1}{2} \left(\frac{K}{|K - 2J|} - 1 \right)^{-1/2}.$$
 (5.9)

In the antiferromagnetic region (J > K/2) , the interaction energy is

$$H_{\text{int}}^{\psi} = \pi J_{\psi}(\tilde{\mu}_{0}^{\psi})^{2} \boldsymbol{m}^{(\alpha)} \cdot [K_{2}(k_{\psi}r_{\alpha\beta})f + K_{0}(k_{\psi}r_{\alpha\beta})\mathbf{1}] \, \boldsymbol{m}^{(\beta)},$$
(5.10)

where the form factor f is defined in eq. (5.5) Its long-range asymptotic form is

$$H_{\text{int}}^{\psi} = \sqrt{\frac{\pi^3}{2k_{\psi}r_{\alpha\beta}}} J_{\psi}(\mu_0^{\psi})^2 e^{-k_{\psi}r_{\alpha\beta}} \boldsymbol{m}^{(\alpha)} \cdot [f-1] \boldsymbol{m}^{(\beta)}.$$
(5.11)

This result shows that, the bilinear coupling of the magnetic moments and the exponential decay of the radial part are common with the ferromagnetic region, but the interaction has anisotropy. Its angular part contains dipole-dipole like anisotropic terms inadition to isotropic and ferromagnetic term.

5.3 Numerical Calculation

We have analytically derived the interaction between impurity magnetic moments, making use of the continuum field theory of the low energy excitation in the bulk region and simplified coupling between each impurity and the bulk. Now we numerically calculate interaction energy, in order to check the validity of these simplifications.

We calculated the ground state energy of a finite-size system with two impurities of L=40 with the fixed boundary condition as explained in §4.2. Here L denotes the number of layers around the origin and impurities are located symmetrically around the origin. Then we determined the interaction energy by subtracting from the ground-state energy one-impurity contributions, which were also derived numerically. We took the limit $J'=-\infty$ and fixed the impurity magnetic moments, for proper comparison with the analytical results in the previous subsection. In addition, we consider the cases $(\boldsymbol{m}^{(\alpha)}, \boldsymbol{m}^{(\beta)}) = (\boldsymbol{m}_A, \boldsymbol{m}_B), \ (\boldsymbol{m}_A, -\boldsymbol{m}_B)$, where $\boldsymbol{m}_A \equiv \frac{1}{\sqrt{3}}(1,1,1), \ \boldsymbol{m}_B \equiv \frac{1}{\sqrt{3}}(1,-1,-1)$.

The analytical results show that the interaction consists of the part mediated by nonmagnetic excitation $H_{\rm int}^{\pi}$, and the part mediated by magnetic excitation $H_{\rm int}^{\psi}$. One remarkable difference between the two parts is that the latter part changes sign, when either spin is reversed, while the former part does not. Using this property, we can separate the nonmagnetic and magnetic parts of the interaction as follows:

$$H_{\text{int}}^{\pi} = \frac{1}{2} \left\{ H_{\text{int}}(\boldsymbol{m}_A, \boldsymbol{m}_B) + H_{\text{int}}(\boldsymbol{m}_A, -\boldsymbol{m}_B) \right\} \quad (5.12)$$

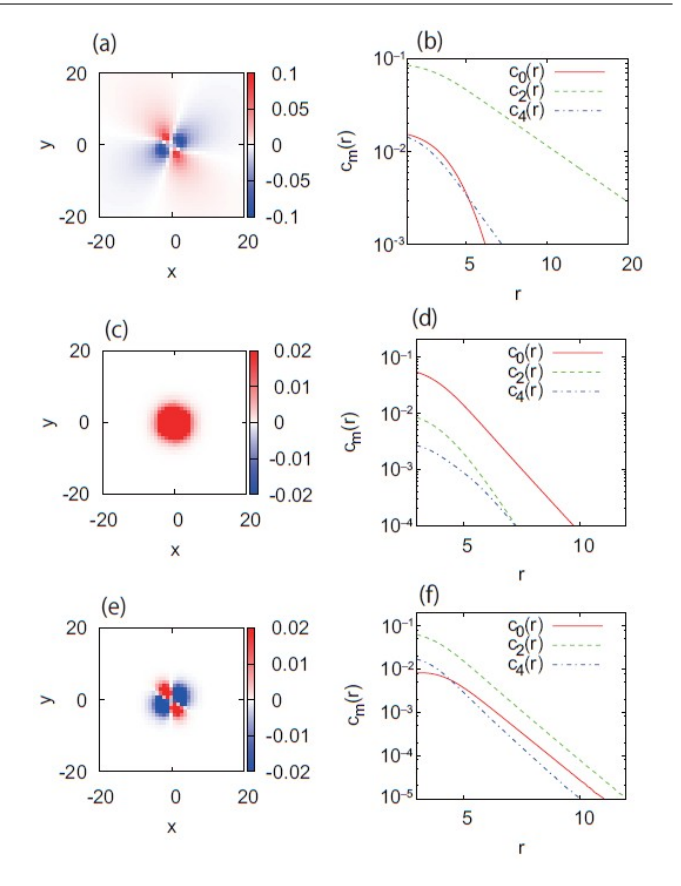


Fig. 12. Distance dependence of (a) nonmagnetic interaction $H_{\rm int}^{\pi}$, and (c)(e) magnetic interaction $H_{\rm int}^{\psi}$. (c) corresponds to J/K=0.1 in the ferromagnetic region and (e) is for J/K=0.9 in the antiferromagnetic region. Corresponding dominant angular-moment components are plotted in log-log scale in (b) and in semi-log scale in (d) and (f).

$$H_{\text{int}}^{\psi} = \frac{1}{2} \left\{ H_{\text{int}}(\boldsymbol{m}_A, \boldsymbol{m}_B) - H_{\text{int}}(\boldsymbol{m}_A, -\boldsymbol{m}_B) \right\} \quad (5.13)$$

Further, to clarify the angular dependence of each part, we performed partial-wave decomposition as $H_{\text{int}}^{\pi(\psi)} = c_0 + \sum_{m=1}^{\infty} c_m \cos\left(m(\theta - \theta_0^{(m)})\right)$.

Let us present the results of these analyses. First, we show the nonmagnetic interaction H_{int}^{π} at J/K = 0.5 in Fig. 12 (a) and (b), where dependence on separation $r_{\alpha\beta}$ and radial dependences of the three large components are shown. We can see that the dipole component $c_2(r)$ decays as r^{-2} , and this is the dominant component. It agrees with the analytical result (5.3). In addition, the principal axis of the angular dependence coincides with that of the analytical result (5.3). Next, we turn to the magnetic interaction $H_{\rm int}^{\psi}$ at J/K = 0.1 in the ferromagnetic region shown in Fig. 12 (c) and (d). The monopole component $c_0(r)$ decays exponentially with separation r, and is dominant, which agrees with the analytical result (5.7). Lastly, the magnetic interaction $H_{\rm int}^{\psi}$ at J/K = 0.9in the antiferromagnetic region is shown in Fig. 12 (e) and (f). The dominant component is now dipole one $c_2(r)$, and the monopole component $c_0(r)$ is of the same order as dipole one but slightly smaller. This agree with the analytical result (5.11), and the ratio of the dipole and monopole components is $c_0/c_2 = 0.34$, at r = 10,

close to the analytical result, 0.41. Again, the principal axes agree with that of the analytical result.

These numerical data show that the analytical results describe the impurity-impurity interactions correctly on qualitative level.

6. Discussion on Spin Freezing

Let us now apply the results in the previous section to discussion on unusual spin freezing observed in NiGa₂S₄. First we discuss the possibility that the long range impurity-impurity interaction, which is mediated by nonmagnetic excitation in the bulk region, causes freezing of the impurity magnetic moments. Based on this scenario of novel spin freezing, second we discuss the anomalies in experiments in NiGa₂S₄ concerning spin freezing, particularly persistent spin dynamics below spin freezing temperature T_f and also scaling behavior of T_f .

Several features shown in our calculations are important to realize unusual spin freezing. We have shown that the anisotropy of impurity magnetic moment and shortrange and long-range impurity-impurity interactions are caused by magnetic and nonmagnetic excitations in the bulk region. The anisotropic long range interaction mediated by nonmagnetic excitation is particularly relevant to the spin freezing. Let us consider the case where impurities are randomly located and their density is small but finite. In this case the spatial anisotropy of the impurityimpurity biquadratic interaction yields randomness and frustration, which are the origins of freezing phenomena. Two other points are important. First, that the biquadratic part of the impurity-impurity interactions are long-ranged and decays as a power law, r^{-2} . Second, the nematic order in the bulk induces spin anisotropy of impurity magnetic moments and effectively spins have only discrete degrees of freedom. Gandolfi et al. studied Ising spins on a hyper cubic lattice with random interactions, and proved that it has a thermodynamical spin glass order at any temperature, if the interaction is sufficiently long-ranged.¹⁹⁾ r^{-2} dependence on two dimensional lattices satisfies this condition. Spin discreteness and long-range interactions are essential factors stabilizing spin glass order in their theory, and our system also shares these two points. Therefore it is reasonable to expect that our system has a similar thermodynamically stable glass order, although the effect of different discrete spin symmetries is not clear. It is an important future issue to prove this expectation. Instead, here let us point out one expected feature of spin freezing. The impurity-impurity interaction is biquadratic with regard to impurity magnetic moments, and therefore is invariant under the local spin inversion of each impurity magnetic moment. One could alternatively say that degrees of freedom involved in the interaction are headless vectors, which are derived from ordinary Heisenberg spins by identifying their two tips. Hence, this interaction should cause the freezing of the headless vectors, rather than original magnetic dipoles. To put it simply, in this freezing state, each impurity magnetic moment fluctuates so that the local expectation value of the dipole moment vanishes, although it tends to be parallel or antiparallel to the local easy axis which is spontaneously chosen.

However, it is necessary to note that the direction of this easy axis is not statically fixed. Throughout this study the coordinate system in the spin space is defined relative to the ordered quadrupole moment in the bulk region as a reference frame. At finite temperatures this reference frame is not static. It fluctuates in the time scale of the autocorrelation time of spin quadrupole moment. Therefore the easy axis of the impurity magnetic moment also fluctuates with the same time scale.

Next we discuss on internal magnetic field below T_f , on the basis of the freezing mechanism just proposed. As we mentioned in §1, μSR experiments revealed the presence of randomly distributed internal magnetic field, which fluctuates with a time scale of μ s, and this dynamics of the internal field is suppressed under magnetic field $H_L \geq 10$ mT. Our scenario can explain the origin of this slow relaxation: that is flip of the impurity magnetic moments along their easy axes. Note that this flipping process without energy cost is a unique result of the biquadratic form of impurity-impurity interaction. This idea can also explain the suppression of the dynamics by magnetic field. The local degeneracy of the two directions of impurity magnetic moment, which correspond to the two tips of the easy axis, is lifted by external magnetic field due to Zeeman energy. Note that not only the impurity magnetic moment but also induced magnetic moments around the impurity, participate in this flipping process. Magnetic moments are induced around an impurity, as we revealed in §4. The radius of this region is the magnetic correlation length, which is divergingly large near the phase boundary, and also experimentally determined as about seven times the lattice constant, as mentioned in §1. Therefore, it is likely that relatively few impurities, for example 1% of the bulk spins, induce the quasi-static magnetic moments and their slow dynamics on most sites, like observed experimentally. It is also a future task to investigate this possibility on more quantitative ground.

Then we present a possible explanation for the scaling behavior of the freezing temperature T_f . As mentioned in $\S 1, T_f$ scales with the characteristic energy scale of the low temperature specific heat upon controlling nonmagnetic impurity concentration. It implies that the freezing occurs simultaneously with some kind of transition

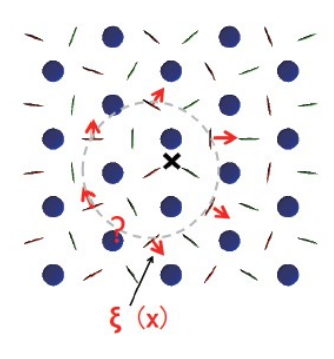


Fig. 13. An example of configuration of spin quadrupole moments around a quaternion vortex excitation in the AFQ order. On the dotted circle, we can not consistently define the coordinate axes, which are parallel to the director on the sublattices.

which is related to the bulk order. One candidate is the vortex unbinding transition. Topologically stable defects exist in the AFQ order, as is shortly discussed in Appendix B, and therefore we expect the existence of a vortex binding-unbinding transition. This transition in the bulk affects impurity-impurity interaction. The AFQ order sets a reference frame of spin coordinate. For example, we defined x-axis as the director on A sublattice. In doing this, we chose one of the two opposite directions, both of which correspond to the same director. Such a choice is arbitrary, but can be done consistently in space. This situation remains unchanged even at finite temperatures if the system is in the vortex binding phase. In this phase vortices exist as bound pairs, and we can neglect their existence, except for the renormalization of the coupling constant, as far as the long range behavior of the system is concerned. The situation drastically changes, on the other hand, in the vortex unbinding phase, where free vortices exist. As shown in Fig. 13, we can not define the coordinate system consistently around a vortex. Therefore the origin of the long range impurityimpurity interaction essentially breaks down in the unbinding phase. Although the present study does not show explicitly yet, it is natural that the interaction becomes short-ranged and the characteristic length scale is the order of the average distance between free vortices. Since it is known that two dimensional systems with short-range random interactions have no thermodynamical glass order, $^{20)}$ we may say that the freezing temperature T_f in our system coincides with the vortex unbinding transition temperature. This is consistent with the observed scaling behavior of T_f , since T_f and the energy scale of the low-temperature specific heat are determined by the characteristic energy of the low-energy excitation in the AFQ order. We need to investigate the finite temperature problem of our system in order to substantiate this idea.

Now we briefly discuss the effect of the quantum fluctuation. One way to include this is spin-wave like approach starting with the deformed nematic order. We can construct a bosonic Hamiltonian in this vacuum with extended Holstein-Primakoff transformation, which is analogous to those adopted for the AFQ ordered system without impurities.⁸⁾ As stated in §2.2, the quantum correction to the interaction energy arises from some exchange process of the bosonic excitations. Even without quantitative investigation, we can predict basic characteristics of this quantum corrections. Reflecting the spontaneous AFQ order, there are gapless Goldstone modes with linear dispersion.⁸⁾ This implies the boson exchange process yields long-range (power-law decay) interactions. Furthermore, near the gapless point the excitations have nonmagnetic character, 8) which indicates the dominant long-range interaction is nonmagnetic one, while magnetic bilinear interactions would be subdominant. Therefore we expect the basic characteristics of the impurityimpurity interaction and also the discussion on spin freezing will not be changed even if we include the quantum corrections to the interaction.

Finally we shortly comment on other open issues. The models in the present study, both of the bilinearbiquadratic model for the bulk part and the triangular bond disorder for the impurity part, are basically phenomenological. Therefore we have to verify these models on a microscopic point of view.

7. Summary

We have studied the effect of triangular-shaped ferromagnetic bond disorder in the S=1 bilinear-biquadratic model on the triangular lattice, in the parameter region where the antiferro quadrupolar order is realized. We have shown that coupling between impurity magnetic moment and magnetic and nonmagnetic excitations in the bulk yields several kinds of anisotropy of impurity magnetic moment, depending on the coupling constant of the bulk. We have also demonstrated the existence of biquadratic, spatially anisotropic and long-range interaction between impurity magnetic moments, and determined their effective coupling constants. This interaction is mediated by nonmagnetic excitation in the bulk. Based on these, we have presented the possibility of glass-like freezing of impurity magnetic moments due to this interaction. This scenario can explain the unusual spin freezing observed in NiGa₂S₄ with persistent spin dynamics and the scaling behavior of freezing temperature with the energy scale of the bulk.

Acknowledgement

The authors thank S. Nakatsuji, K. Ueda and A. V. Chubukov for stimulating discussions. This study was supported by Grant-in-Aid for Scientific Research on Priority Areas "Novel States of Matter Induced by Frustration" (19052003).

Appendix A: Extension to General Configuration of Impurities

In $\S 4$ and $\S 5$ we have considered the case that an the impurity occupies the position E in Fig. 4. Here we show results for the other positions. One impurity problem is explained in A.1 and impurity interactions are given in A.2 for general cases of pair configuration.

A.1 One Impurity Problem

Here we extend the calculation of the ground state field configuration around a single impurity in §4.2 and §4.3, when the impurity occupies a general position in Fig. 4.

As for the nonmagnetic part, the ground state configuration of nonmagnetic excitation π is given by eq. (4.13) and (4.17), for the configuration E in Fig. 4. For example, in the case of C_3 , we can obtain the ground state by $\frac{2}{3}\pi$ rotation in real space from that in the case of E. This corresponds to the change of the lattice vectors as $\hat{\kappa}_1 \to \hat{\kappa}_2$, $\hat{\kappa}_2 \to \hat{\kappa}_3$, $\hat{\kappa}_3 \to \hat{\kappa}_1$. The other cases are also similarly obtained. It is natural to relate the configurations of the impurity, to the elements of the trigonal point group $C_{3v} = \{E, C_3, C_3^{-1}, \sigma_1, \sigma_2, \sigma_3\}$. That is why we introduced the notation for the configuration.

Taking advantage of this relationship, the general expression for the dipole moment (4.17) is given as:

$$\boldsymbol{\mu}_a^{\pi} = \mu_0^{\pi} \sum_{b,c} \frac{|\epsilon_{abc}|}{2} m_b m_c \hat{\kappa}_a^h, \tag{A.1}$$

where $h \in C_{3v}$ denotes the impurity position and

$$\begin{pmatrix} \hat{\kappa}_{1}^{h} \\ \hat{\kappa}_{2}^{h} \\ \hat{\kappa}_{3}^{h} \end{pmatrix} = D_{h} \begin{pmatrix} \hat{\kappa}_{1} \\ \hat{\kappa}_{2} \\ \hat{\kappa}_{3} \end{pmatrix}. \tag{A.2}$$

Here D_h is a three-dimensional representation of C_{3v} :

$$D_{E} = \begin{pmatrix} 1 & 0 & 0 \\ 0 & 1 & 0 \\ 0 & 0 & 1 \end{pmatrix}, D_{C_{3}} = \begin{pmatrix} 0 & 1 & 0 \\ 0 & 0 & 1 \\ 1 & 0 & 0 \end{pmatrix}$$

$$D_{C_{3}^{-1}} = \begin{pmatrix} 0 & 0 & 1 \\ 1 & 0 & 0 \\ 0 & 1 & 0 \end{pmatrix}, D_{\sigma_{1}} = \begin{pmatrix} 1 & 0 & 0 \\ 0 & 0 & 1 \\ 0 & 1 & 0 \end{pmatrix}$$

$$D_{\sigma_{2}} = \begin{pmatrix} 0 & 0 & 1 \\ 0 & 1 & 0 \\ 1 & 0 & 0 \end{pmatrix}, D_{\sigma_{3}} = \begin{pmatrix} 0 & 1 & 0 \\ 1 & 0 & 0 \\ 0 & 0 & 1 \end{pmatrix}.$$

$$(A\cdot3)$$

The magnetic part can be calculated similarly and we show only results. Ground state configuration of magnetic field ψ is given by eq. (4.28), and monopole and dipole moments are given as

$$q_a^{\psi} = q_0^{\psi} m_a, \quad \boldsymbol{\mu}_a^{\psi} = \mu_0^{\psi} m_a \hat{\boldsymbol{\kappa}}_a^{'h}, \quad (J < K/2) \quad (A\cdot 4)$$

$$q_a^{\psi} = 0, \quad \boldsymbol{\mu}_a^{\psi} = \tilde{\mu}_0^{\psi} m_a \hat{\boldsymbol{\kappa}}_a^h, \qquad (J > K/2), \quad (A.5)$$

where we defined

$$\begin{pmatrix} \hat{\kappa}_{1}^{'h} \\ \hat{\kappa}_{2}^{'h} \\ \hat{\kappa}_{3}^{'h} \end{pmatrix} = \sigma_{h} D_{h} \begin{pmatrix} \hat{\kappa}_{1}^{'} \\ \hat{\kappa}_{2}^{'} \\ \hat{\kappa}_{3}^{'} \end{pmatrix}. \tag{A-6}$$

 D_h denotes the three dimensional representation of C_{3v} introduced by eq. (A·3), and σ_h denotes A_2 representation of C_{3v} : $\sigma_E = \sigma_{C_3} = \sigma_{C_3^{-1}} = 1$, $\sigma_{\sigma_1} = \sigma_{\sigma_2} = \sigma_{\sigma_3} = -1$.

Note that the ground state energy is independent of the impurity position for both nonmagnetic and magnetic parts.

A.2 Interaction between Impurities

Using the results of the previous subsection, we can calculate the interaction energy for general cases of impurity pair configuration. The impurity α occupies the position h_{α} , while the partner impurity β occupies the position h_{β} in a unit cell far away from the impurity α . As for the nonmagnetic part, the interaction energy is

$$H_{\text{int}}^{\pi} = \pi J_{\pi} \frac{r_0^2 (\mu_0^{\pi})^2}{r_{\alpha\beta}^2} \text{Tr} \left(T^{(\alpha)} f_{h_{\alpha} h_{\beta}} T^{(\beta)} \right) \tag{A.7}$$

$$(f_{h_{\alpha}h_{\beta}})_{ab} = \left\{ D_{h_{\alpha}} \left[D_{\sigma_1} \cos(2\theta + \frac{2\pi}{3}) + D_{\sigma_2} \cos(2\theta - \frac{2\pi}{3}) \right] \right\}$$

$$+D_{\sigma_3}\cos 2\theta]D_{h_{\beta}}^T\Big\}_{ab}\delta_{ab},$$
 (A·8)

where matrices $T^{(x)}$, $(x = \alpha, \beta)$ are defined in eq. (5.4). We can see that principal axes of dipole-dipole like anisotropy depend on the position of impurity pair, but the interaction has the same form as before.

As for the magnetic part in the ferromagnetic region, interaction energy (5.6) is independent of impurity pair configuration. In the antiferromagnetic region, the inter-

Table B·1. Class multiplication table for the quaternion group, Ω

| | C_0 | \overline{C}_0 | C_x | C_y | C_z |
|------------------|------------------|------------------|--------------------------|--------------------------|--------------------------|
| | | | C_x | C_y | C_z |
| \overline{C}_0 | \overline{C}_0 | C_0 | C_x | C_y | C_z |
| C_x | C_x | C_x | $2C_0 + 2\overline{C}_0$ | $2C_z$ | $2C_y$ |
| | | | $2C_z$ | $2C_0 + 2\overline{C}_0$ | $2C_x$ |
| | | | $2C_y$ | $2C_x$ | $2C_0 + 2\overline{C}_0$ |

action energy (5.10) is replaced by the general expression

$$H_{\text{int}}^{\psi} = \pi J_{\psi}(\tilde{\mu}_{0}^{\psi})^{2} \boldsymbol{m}^{(\alpha)} \cdot \left[K_{2}(k_{\psi}r_{\alpha\beta}) f_{h_{\alpha}h_{\beta}} + K_{0}(k_{\psi}r_{\alpha\beta}) \mathbf{1} \right] \boldsymbol{m}^{(\beta)}. \tag{A.9}$$

Again, difference of impurity pair configuration is reflected only in the change of principal axes of dipole-dipole like anisotropy.

Appendix B: Topological Excitation in Antiferro Quadrupolar Order

In §3 we mentioned the presence of topological excitations in the AFQ order, and it is closely related to the mechanism of spin freezing transition presented in §6. Here we briefly summarize the properties of these topological excitations. Detailed general arguments on topological excitations may be found, for example, in the review by Mermin.²¹⁾ In our context, topological excitations mean defects in static configuration of the order parameter which is not removable by any continuous transformation of configuration.²²⁾

Since the system of our concern is two-dimensional, relevant topological excitations are point defects. They can not be removed by continuous transformation of local order parameters inside a contour enclosing the defect. The simplest example for this is a vortex in ferromagnetically ordered XY spins and this is characterized by an integer winding number. Only defects with the same winding number can be continuously deformed to each other. In general ordered media, a simple winding number is not sufficient to label a defect, but one can use the homotopy theory. For order parameter space R, one defines the fundamental group $\pi_1(R)$, which is generally not Abelian, and a topological defect can be labeled by one of its conjugacy classes.

Order parameter space of the AFQ state is more complicated than simple cases like ferromagnetic order of XY spins. This is generally defined as the coset group G/H, where G is the symmetry group that keeps the original Hamiltonian invariant, while H is its subgroup that keeps the ordered state invariant. The bilinear-biquadratic model (1.1) has a complete spherical symmetry in spin space and the time reversal symmetry. Therefore G is $SO(3) \times Z_2$. The AFQ state is invariant under 180° rotations about three mutually perpendicular axes, which form the dihedral group D_2 of order 4, and also the time reversal operation. Therefore the order parameter space is $R = (SO(3) \times Z_2)/(D_2 \times Z_2) = SO(3)/D_2$ or equivalently SU(2)/Q, where Q is the quaternion group. It is order 8 and non-Abelian, and has a two-dimensional

representation:

$$\mathbf{Q} = \{\mathbf{1}, -\mathbf{1}, i\sigma_x, -i\sigma_x, i\sigma_y, -i\sigma_y, i\sigma_z, -i\sigma_z\}, \quad (\mathbf{B} \cdot \mathbf{1})$$

where $\sigma_a(a=x,y,z)$ are the Pauli matrices.

It is known that for a continuous and simply connected group G, with a discrete subgroup H, the fundamental group of G/H is $\pi_1(G/H) = H.^{21}$ In our case, G is the rotation group SU(2) and H is the quaternion group Q, and therefore the fundamental group of our order parameter space is $\pi_1(R = SU(2)/Q) = Q$. Note that SU(2) is a simply connected group but SO(3) is not. Topological defects are thus classified by its five conjugacy classes as:²¹⁾

$$C_0 = \{1\}, \ \overline{C}_0 = \{-1\},$$

 $C_x = \{\pm i\sigma_x\}, \ C_y = \{\pm i\sigma_y\}, \ C_z = \{\pm i\sigma_z\},$ (B·2)

including C_0 corresponding to no topological defect. Note that three conjugacy classes contain multiple elements of Q. This is the result of non-Abelian nature of the group Q.

The non-Abelian nature of the fundamental group Q implies nontrivial merging rules of topological defects. Consider two defects and what happens if we merge them. The point is non-uniqueness of the defect class for the merged defect. To define the defect class for the merged ones, one needs a closed path which encloses these two. The answer follows the class multiplication table for $\pi_1(R) = Q$ shown in Table B·1. Note that some products contain more than one classes, reflecting non-commutative nature of the group Q. For that case, the answer depends on the configurations of other defects, if present. Typical cases are shown in Fig. B·1 and the two paths both enclose the same two defects but they may yield different classes for the merged defect.

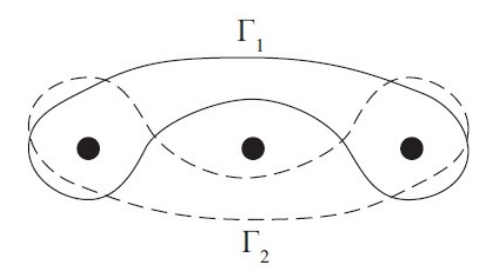


Fig. B·1. Two contours Γ_1 and Γ_2 enclosing two defects going through the opposite sides of the third defect. Defects are shown by black circles.

- A. P. Ramirez: in *Handbook of Magnetic Materials*, ed. K. J. H. Buschow (Elsevier Science, Amsterdam, 2001) vol. 13, p. 423.
- 2) H. T. Diep: Magnetic system with competing interactions (frustated spin systems), (World Scientific, Singapore, 1994).
- 3) P. W. Anderson: Matter. Res. Bull. 8 (1973) 153.
- B. Bernu, P. Lecheminant, C. Lhuillier, and L. Pierre: Phys. Rev. B 50 (1994) 10048.
- Y. Shimizu, K. Miyagawa, K. Kanoda, M. Maesato, and G. Saito: Phys. Rev. Lett. 91 (2003) 107001.
- S. Nakatsuji, Y. Nambu, H. Tonomura, O. Sakai, S.Jonas, C. Broholm, H.Tsunetsugu, Y. Qiu and Y. Maeno: Science 309 (2005) 1697.
- A. P. Ramirez, G. P. Espinosa and A. S. Cooper: Phys. Rev. Lett. 64 (1990) 2070.
- H. Tsunetsugu and M. Arikawa: J. Phys. Soc. Jpn. 75 (2006) 083701
- A. Läuchli, F. Mila, and K. Penc: Phys. Rev. Lett. 97 (2006) 087205.
- 10) D. E. MacLaughlin, Y. Nambu, S. Nakatsuji, R. H. Heffner, Lei Shu, O. O. Bernal, and K. Ishida: Phys. Rev. B 78 (2008) 220403(R).
- Y. Nambu, S. Nakatsuji, Y. Maeno, E. K. Okudzeto, and J. Y. Chan: Phys. Rev. Lett. 101 (2008) 207204.
- Y. Nambu, R. T. Macaluso, T. Higo, K. Ishida, and S. Nakatsuji: Phys. Rev. B 79 (2009) 214108.
- B. A. Ivanov and A. K. Kolezhuk: Phys. Rev. B 68 (2003) 052401.
- S. Sachdev: Quantum Phase Transitions (Cambridge University Press, Cambridge, England, 1999)p.240.
- A. Polyakov and P. B. Wiegmann, Phys. Lett. **131B** (1983)
 121.
- 16) The 2-dimensional classical models (3.13) and (3.19) describe energy cost associated with static deformation of nonmagnetic and magnetic local order parameters. They describe different physics than the one in Ref.15, where the (1+1)-dimensional action describes quantum mechanical dynamics in space and time.
- 17) N. D. Mermin and H. Wagner: Phys. Rev. Lett. 17 (1966) 1133.
- G. B. Arfken and H. J. Weber: Mathematical methods for physicists (Elsevier Academic Press, Amsterdam, 2005).
- A. Gandolfi, C. M. Newman, and D. L. Stein: Commun. Math. Phys. 157 (1993) 371.
- P. W. Anderson, and C. W. Pond: Phys. Rev. Lett. 40 (1978)
- 21) N. D. Mermin: Rev. Mod. Phys. **51** (1979) 591.
- 22) Topological defects may exist also in the (d+1)-dimensional effective action of a d-dimensional quantum Hamiltonian and might change the character of quantum mechanical excitation spectrum drastically. In the AFQ order, however, this type of topological defects are absent. This is because the space-time dimension is now 3 and one needs to examine the third homotopy group π_3 , which is trivial for the order parameter space SU(2)/Q.